Reactive metabolic byproducts contribute to antibiotic lethality under anaerobic conditions

Citation: Wong, Felix, Stokes, Jonathan M, Bening, Sarah C, Vidoudez, Charles, Trauger, Sunia A et al. 2022. "Reactive metabolic byproducts contribute to antibiotic lethality under anaerobic conditions." Molecular Cell, 82 (18).

As Published: 10.1016/j.molcel.2022.07.009

Publisher: Elsevier BV

Persistent URL: https://hdl.handle.net/1721.1/147987

Version: Author's final manuscript: final author's manuscript post peer review, without publisher's formatting or copy editing

Reactive metabolic byproducts contribute to antibiotic lethality under anaerobic conditions

Felix Wong[1,2], Jonathan M. Stokes[1,2,#], Sarah C. Bening[1,2], Charles Vidoudez[3], Sunia A. Trauger[3], and James J. Collins[1,2,4,5,*]

[1]Institute for Medical Engineering & Science and Department of Biological Engineering, Massachusetts Institute of Technology, Cambridge, MA 02139, USA

[2]Infectious Disease and Microbiome Program, Broad Institute of MIT and Harvard, Cambridge, MA 02142, USA

[3]Harvard Center for Mass Spectrometry, Harvard University, Cambridge, MA 02138

[4]Wyss Institute for Biologically Inspired Engineering, Harvard University, Boston, MA 02115, USA

[5]Lead contact

*Correspondence to: James J. Collins (jimjc@mit.edu)

[#]Current address: Department of Biochemistry and Biomedical Sciences, Michael G. DeGroote Institute for Infectious Disease Research and David Braley Centre for Antibiotic Discovery, McMaster University, ON L8S 4L8, Canada

Summary

Understanding how bactericidal antibiotics kill bacteria remains an open question. Previous work has proposed that primary drug target corruption leads to increased energetic demands, resulting in the generation of reactive metabolic byproducts (RMBs), particularly reactive oxygen species, that contribute to antibiotic-induced cell death. Studies have challenged this hypothesis by pointing to antibiotic lethality under anaerobic conditions. Here, we show that treatment of *Escherichia coli* with bactericidal antibiotics under anaerobic conditions leads to changes in the intracellular concentrations of central carbon metabolites, as well as the production of RMBs, particularly reactive electrophilic species (RES). We show that antibiotic treatment results in DNA double-strand breaks and membrane damage, and demonstrate that antibiotic lethality under anaerobic conditions can be decreased by RMB scavengers, which reduce RES accumulation and mitigate associated macromolecular damage. This work indicates that RMBs, generated in response to antibiotic-induced energetic demands, contribute in part to antibiotic lethality under anaerobic conditions.

INTRODUCTION

Elucidating how bactericidal antibiotics kill bacteria remains a central problem in microbiology (Kohanski et al. 2010a). While the primary binding targets of antibiotics have been characterized, how bacterial cell death occurs as a result of primary binding interactions remains unclear. We have previously hypothesized that the induction of stress response pathways to alleviate the deleterious consequences of the initial target corruption leads to increased energetic demands that heighten metabolic activity (Kohanski et al. 2007; Dwyer et al. 2007; Lobritz et al. 2016; Stokes et al. 2019). Increased metabolic flux results in the production of reactive metabolic byproducts (RMBs), including but not limited to reactive oxygen species (ROS), that contribute to antibiotic lethality by reacting with and damaging cellular components downstream of antibiotic binding to the primary target (Kohanski et al. 2007; Stokes et al. 2019; Belenky et al. 2015; Foti et al. 2012). The feedback between damage to macromolecules, increased metabolic flux, and production of RMBs persists until bacterial cell death occurs (Stokes et al. 2019).

This hypothesis has been supported by multiple laboratories using independent lines of evidence (Gusarov et al. 2009; Wang et al. 2009; Davies et al. 2009; Yeom et al. 2010; Shatalin et al. 2011; Nguyen et al. 2011; Luo et al. 2012; Dwyer et al. 2012; Grant et al. 2012; Brynildsen et al. 2013; Moronez-Ramirez et al. 2013; Hong et al. 2019; Drlica et al. 2020). It also has been challenged by other studies based on the argument that antibiotic killing of *Escherichia coli* in aerobic and anaerobic conditions can be similar (Keren et al. 2013; Liu et al. 2013), and ROS are ostensibly not generated under anaerobic conditions. However, it is important to point out that the above mechanistic model does not assume or purport that ROS are the sole arbiters of antibiotic lethality. Moreover, the induction of stress response pathways as a result of corruption of the primary drug target and its associated cellular processes, as well as the resulting energetic demands that heighten metabolic activity, may not be exclusive to aerobic conditions.

Building on the foregoing points, we hypothesize that, under anaerobic conditions, bactericidal antibiotics corrupt target-specific cellular processes and result in increased energetic demands similar to those previously described under aerobic conditions (Kohanski et al. 2007). As a result of increased metabolic flux through anaerobic energy-producing processes (e.g., fermentation and anaerobic respiration with non-oxygen terminal electron acceptors, including nitrate, sulfate, and ferric iron) and additional processes such as free radical interactions, diverse RMBs are produced and these RMBs promiscuously react with, and disrupt, cellular

components, leading to macromolecular damage that contributes in part to antibiotic lethality. This hypothesis implies that, while specific aspects—including which metabolic pathways experience altered flux and which RMBs are subsequently generated—may vary between anaerobic and aerobic conditions, RMBs contribute in part to antibiotic lethality under both conditions.

Here, we aimed to test this hypothesis by determining whether RMBs may contribute to antibiotic lethality under anaerobic conditions. To this end, we used a combination of single-cell assays, bulk culture measurements, and biochemical perturbations to examine how antibiotics affect the metabolic states of treated cells and how RMBs may contribute to antibiotic lethality under anaerobic conditions. As in previous work (Kohanski et al. 2007; Keren et al. 2013; Liu et al. 2013), we focus here on three main classes of bactericidal antibiotics: aminoglycosides, which bind to the 30S ribosomal subunit and induce protein mistranslation; fluoroquinolones, which bind to DNA gyrase or topoisomerase to perturb DNA replication and transcription; and β-lactams, which bind penicillin-binding proteins to disrupt peptidoglycan cell wall biosynthesis. We show that treatment of *Escherichia coli* with these three classes of antibiotics under anaerobic conditions leads to alterations in the cellular concentrations of central carbon metabolites, including glucose, pyruvate and NADH/NAD^+. By employing single-cell microscopy and specific gas chromatography-mass spectrometry (GC-MS) experiments, we also find that reactive metabolic byproducts, particularly reactive electrophilic species, accumulate in antibiotic-treated *E. coli* under anaerobic conditions. At the single-cell level, we show that antibiotic treatment results in DNA double-strand breaks and membrane damage, consistent with the hypothesis that macromolecular damage can be induced in part by reactive electrophilic species. Importantly, we demonstrate that antibiotic lethality is decreased by three different reactive metabolic byproduct scavengers—glutathione, acetylcysteine, and pyridoxamine—which reduce reactive electrophilic species accumulation and mitigate the macromolecular damage induced by antibiotics under anaerobic conditions. This work indicates that in the absence of environmental oxygen, antibiotic-induced changes in cellular metabolism result in the production of RMBs that promiscuously react with cellular components, resulting in macromolecular damage which contributes in part to antibiotic lethality.

RESULTS

Antibiotic lethality occurs under anaerobic conditions

To determine the extent to which antibiotic killing occurs under anaerobic conditions, we treated bulk cultures of log-phase *E. coli* with the aminoglycoside kanamycin, the fluoroquinolone ciprofloxacin, and the β-lactam mecillinam at concentrations ranging from 0.1× to 50× the anaerobic minimum inhibitory concentrations (MICs; Table S1). Cells were grown, treated, plated, and incubated under anaerobic conditions in LB medium containing resorufin, an oxygen-sensitive dye which is colorless below a redox potential of -110 mV and used here to validate the absence of environmental oxygen. The addition of resorufin is important, as an anaerobic environment, by itself, can be insufficient to deprive culture media of oxygen. Under these conditions, time-kill assays and colony-forming unit (CFU) quantitation of antibiotic-treated cultures revealed that killing occurred for all three antibiotics, leading to between 0 and ~6 logs of decreased survival depending on antibiotic class, antibiotic concentration, and treatment time (Figure 1A). We observed similar levels of decreased survival under aerobic conditions, with the exception of treatment with mecillinam, for which at most ~1 log of decreased survival occurred (Figure S1). These findings indicate the extents to which antibiotic killing occurs in LB medium under anaerobic and aerobic conditions, and are similar to the findings of previous studies (Keren et al. 2013; Liu et al. 2013).

Antibiotic treatment results in altered central carbon metabolite concentrations under anaerobic conditions

As antibiotic lethality occurs under anaerobic conditions, we hypothesized that, under such conditions, bactericidal antibiotics corrupt target-specific cellular processes and result in increased energetic demands similar to those previously described under aerobic conditions (Kohanski et al. 2007). Under anaerobic conditions, *E. coli* can generate ATP through glycolysis, which converts glucose into pyruvate, resulting in the generation of ATP and NADH, and anaerobic respiration with non-oxygen terminal electron acceptors, which oxidizes NADH to replenish NAD^+ (Figure 1B). In order to determine whether intracellular concentrations of central carbon metabolites are altered after antibiotic treatment, we measured glucose, pyruvate, and NADH/NAD^+ concentrations in antibiotic-treated cells using enzymatic assays. We treated log-phase bulk cultures with kanamycin, ciprofloxacin, and mecillinam at concentrations ranging

from 1× to 50× the anaerobic MICs under anaerobic conditions and harvested cells after a treatment time of 20 min, similar to previous work examining changes in metabolic flux in antibiotic-treated cells under aerobic conditions (Kohanski et al. 2007; Belenky et al. 2015). We found that endogenous concentrations of glucose were increased in antibiotic-treated cell cultures relative to untreated controls (Figure 1C). Cells treated with kanamycin, ciprofloxacin, and mecillinam across a range of low (1× MIC) and high (5× to 50× MIC) concentrations exhibited average glucose concentrations that were as large as 4-fold that of untreated cells. Intriguingly, cells treated with mecillinam at a high (50× MIC; 10 μg/mL) concentration exhibited lower glucose concentrations compared to treatment at a low mecillinam concentration; why this occurs is unclear, but it is possible that extensive primary target corruption at high mecillinam concentrations may dominate the cellular response to the antibiotic under these conditions.

Building on the above measurements of glucose concentrations, we next measured pyruvate and NADH/NAD^+ concentrations. We reasoned that, as pyruvate is an end-product of glycolysis, pyruvate accumulation may indicate increased glycolytic flux (Zhu et al. 2008). Additionally, alterations to NADH/NAD^+ concentration ratios may lead to redox imbalance and increased RMB production (Kohanski et al. 2007). We found increased concentrations of pyruvate similar to glucose (Figure 1D): average pyruvate levels in antibiotic-treated cells were between ~1.5 to ~4-fold that of untreated cells, and treatment with mecillinam at a high concentration resulted in lower pyruvate accumulation compared to treatment at a low concentration (similar to what was found for glucose). Measuring NADH/NAD^+ concentration ratios, we found that average NADH/NAD^+ ratios in antibiotic-treated cells were between ~0.5 to ~1.2-fold that of untreated cells (Figure 1E). Treatment with kanamycin at a high (5× MIC; 250 μg/mL) concentration and mecillinam at a low (1× MIC; 0.2 μg/mL) concentration increased average NADH/NAD^+ concentrations relative to non-treatment conditions, while average NADH/NAD^+ concentrations were decreased for all other treatment conditions. These measurements suggest that, under different treatment conditions, NADH might be differentially altered by processes including anaerobic respiration and fermentation on the timescale of interest. In general, NADH/NAD^+ concentrations changed to a lesser extent than those of glucose and pyruvate, which may reflect better NADH/NAD^+ homeostasis (Figure 1B).

Taken together, the above results indicate largely altered glucose, pyruvate, and/or

NADH/NAD^+ concentrations in antibiotic-treated *E. coli* relative to untreated controls. These findings suggest that antibiotic treatment may result in alterations to cellular metabolism, wherein increased ATP demand as a result of primary target corruption leads to increased central carbon metabolism through catabolic processes including glycolysis. Importantly, increased metabolism may result in the formation of RMBs: these include methylglyoxal, a reactive electrophilic species which is generated as a byproduct of glycolysis, and various RMBs that arise as a consequence of the oxidation of NADH to NAD^+ and the reduction of terminal electron acceptors (Figure 1B).

Phenotypic changes and fluorescence of reactive metabolic byproduct-sensitive dyes occur under anaerobic conditions

As a result of increased metabolism in antibiotic-treated cells, we hypothesized that the production of RMBs is associated with antibiotic lethality. To address this, we characterized cellular phenotypes at the single-cell level using microscopy and fluorescent dyes that are sensitive to RMBs and RMB-mediated cellular damage. We have recently used a single-cell approach to show that cytoplasmic condensation, a phenotype in which discrete portions of the cytoplasm become phase-light when imaged under phase-contrast, is associated with cell death in a fraction of cells treated with aminoglycosides or fluoroquinolones (Wong et al. 2021a). In contrast, β-lactams induce well-studied phenotypes of membrane bulging and lysis (Yao et al. 2012; Wong et al. 2019; Wong et al. 2021b). Under aerobic conditions, cytoplasmic condensation and/or cellular lysis are associated with membrane damage, cessation of growth at the single-cell level, and the accumulation of ROS, nitric oxide, and lipid peroxidation adducts, as measured by the fluorescent dyes carboxy-H_2DCFDA, DAF-FM, and C11-BODIPY, respectively (Wong et al. 2021a). We have previously observed that kanamycin- or ciprofloxacin-treated cells irreversibly cease to elongate as soon as they exhibit cytoplasmic condensation (Wong et al. 2021a). Furthermore, the fraction of cells exhibiting cytoplasmic condensation in antibiotic-treated populations are reduced in the presence of glutathione, an antioxidant and cellular detoxifier which also decreases antibiotic lethality (Wong et al. 2021a). Here, under anaerobic conditions, we found that treatment with kanamycin or ciprofloxacin induced cytoplasmic condensation after 4 h of treatment, a timescale corresponding to decreases of at least ~2 logs in survival in bulk culture (Figure 2A and Figure 2B; Figure 1A). Moreover,

183 treatment with all three antibiotics (kanamycin, ciprofloxacin, mecillinam) induced significant,
184 phenotype-dependent increases in fluorescence of carboxy-H_2DCFDA, DAF-FM, and C11-
185 BODIPY in most cells, with typical fluorescence increases being associated with condensation
186 and/or lysis in kanamycin- and ciprofloxacin-treated cells, and with membrane bulging and/or
187 lysis in mecillinam-treated cells (Figures 2C-F). More limited fluorescence increases, especially
188 of C11-BODIPY, occurred as soon as 30 min after antibiotic treatment and well before cells
189 exhibited cytoplasmic condensation, membrane bulging, and lysis, suggesting that the generation
190 of certain RMBs precedes cellular phenotypic changes (Figure S2). Importantly, these
191 fluorescence increases did not arise from oxygen contamination, as resorufin remained strictly
192 colorless throughout our experiments. Taken together, these single-cell assays suggest that
193 RMBs accumulate in antibiotic-treated cells under anaerobic conditions.

194 **Antibiotics induce the production of reactive electrophilic species under anaerobic**
195 **conditions**

196 In addition to arising from molecular oxygen, RMBs, including ROS and non-ROS free radicals,
197 may arise under anaerobic conditions from endogenous sources including NADPH oxidases
198 (Hajjar et al. 2017) and reactive nitrogen species (RNS) synthases (Crane et al. 2010), from
199 anaerobic respiration with terminal electron acceptors including nitrate, sulfate, and ferric iron,
200 and from glycation reactions involving amino acids (Yim et al. 1995). Our observations of
201 cytoplasmic condensation (indicative of membrane damage) and lipid peroxidation (as assayed
202 by C11-BODIPY) suggest that RMBs might directly react with membrane lipids, a process
203 known to produce highly promiscuous and deleterious reactive electrophilic species (RES; Yin et
204 al. 2011). Therefore, we focused on RES, which may be produced anaerobically and aerobically
205 by processes including glycolysis (Ferguson et al. 1999) and lipid peroxidation in bacteria (Yin
206 et al. 2011). RES are biomarkers of RNS-, ROS-, and other free radical-induced macromolecular
207 damage, and RES also stimulate the production of other reactive byproducts including advanced
208 glycation end-products (AGE) and advanced lipoxidation end-products (ALE) through reactions
209 with nucleic acids, proteins, and lipids (Note S1). Examples of RES include 4-hydroxynonenal
210 (4-HNE), a byproduct of lipid peroxidation, and methylglyoxal (MGO), a byproduct of
211 glycolysis and lipid peroxidation. These aldehydes bind cellular components, contribute to
212 mutagenesis, and, in the case of MGO, accumulate in millimolar quantities within cells during

unbalanced sugar metabolism (Ferguson et al. 1999). Under aerobic conditions, we have previously shown that bactericidal antibiotics elevate central carbon metabolism (Yang et al. 2019), and a recent study has suggested that glycolysis contributes to β-lactam killing of Gram-positive bacteria (Kawai et al. 2019). Consistent with these and other works (Dwyer et al. 2014; Wong et al. 2021a), we hypothesized that bactericidal antibiotics kill bacteria under anaerobic conditions in part through the generation of RES and the subsequent reactions of RES with cellular components.

To investigate this hypothesis in anaerobic bulk culture, we measured RES concentrations in log-phase cells treated with antibiotics. Using gas chromatography-mass spectrometry (GC-MS), a standard for analyte detection, we employed a method in which 4-HNE and MGO concentrations at the time of harvest could be assayed after derivatization with *O*-(2,3,4,5,6-pentafluorobenzyl)hydroxylamine (PFBHA; Luo et al. 1995) (Figure S3). Cells were harvested after treatment with antibiotics across a range of concentrations, from 1× to 50× the anaerobic MICs, at an antibiotic treatment endpoint of 2 h. We found that 4-HNE and MGO were present in lysates of cells treated with kanamycin, ciprofloxacin, or mecillinam under anaerobic conditions (Figure 3A and Figure 3B). Furthermore, our measurements suggested that increased antibiotic concentrations resulted in increased average concentrations of 4-HNE and MGO for kanamycin and mecillinam. Ciprofloxacin treatment at higher concentrations (5× MIC; 0.1 μg/mL) did not induce elevated levels of either RES after 2 h relative to treatment at lower concentrations. It is possible that extensive primary target damage and/or simultaneous inhibition of protein synthesis may affect the production of RMBs, including RES, at high ciprofloxacin concentrations, as previously suggested (Drlica et al. 2020). Nevertheless, for all other treatment groups, these measurements indicate that RES are present and may accumulate in antibiotic-treated cells under anaerobic conditions (Figure 3A and Figure 3B). Additionally, increased 4-HNE (but not MGO) concentrations were detectable in cell lysates as early as 30 min after antibiotic treatment (Figure S3), suggesting that the generation of certain RES may occur rapidly after antibiotic treatment.

Next, to understand the physiological effects of RES on cells, we measured cellular survival after exogenous treatment with millimolar concentrations of 4-HNE and MGO (Figure S4). We found that addition of either 4-HNE or MGO led to between 0 to ~6 logs of decreased survival in log-phase cells depending on concentration and treatment time, and lethality occurred

under both anaerobic and aerobic conditions (Figures S4 and S5). Strikingly, consistent with our phenotypic observations for kanamycin and ciprofloxacin treatments (Figure 2A and Figure 2B), single-cell observations reveal that bactericidal concentrations of 4-HNE or MGO also induce cytoplasmic condensation and cellular lysis (Figure S4). Together, these observations qualitatively indicate that, under anaerobic conditions, RES are deleterious to bacterial cells and could contribute in part to the cell death phenotypes observed after antibiotic treatment.

Antibiotic-treated cells display macromolecular damage consistent with damage induced by reactive electrophilic species under anaerobic conditions

Previous studies have shown that, under aerobic (Belenky et al. 2015; Foti et al. 2012; Dwyer et al. 2012; Hong et al. 2019; Dwyer et al. 2014; Wong et al. 2021a) and anaerobic (Wong et al. 2021a; Giroux et al. 2017) conditions, antibiotics induce macromolecular damage distinct from the damage induced by their primary drug target binding activity. Here, we asked whether macromolecular damage also occurs under the anaerobic conditions considered here, and if so, whether it is consistent with our finding that antibiotic-treated cells generate RES. We focused specifically on two markers of macromolecular damage, DNA double-strand breaks and membrane damage. We note that kanamycin and mecillinam can damage cellular membranes through nonspecific ionic interactions (Martin et al. 1986) and primary target binding to penicillin-binding proteins (Yao et al. 2012; Wong et al. 2019; Wong et al. 2021b), respectively, while ciprofloxacin damages DNA by binding to its primary targets of DNA gyrase and topoisomerase. Nevertheless, the accumulation of RES may further contribute to DNA and membrane damage in antibiotic-treated cells. We measured the frequencies of DNA double-strand breaks and membrane damage in antibiotic-treated cells using an engineered fluorescent protein-based probe (GamGFP; Shee et al. 2013) and SYTOX Blue, a membrane damage-sensitive dye, respectively.

Using a GamGFP strain of *E. coli*, we found that cells exhibited DNA double-strand breaks—as manifested by the appearance of fluorescent GFP foci—after treatment with kanamycin, ciprofloxacin, or mecillinam under anaerobic conditions (Figure 3C and Figure 3D). While GFP fluorescence is typically quenched under anaerobic conditions, our observations of GamGFP foci suggest that, under the anaerobic conditions used here, there remains enough oxygen for fluorophore maturation. This suggestion is supported by previous work that has

shown GFP fluorophore maturation even under conditions of 0.1 PPM dissolved oxygen (Hansen et al. 2001), a level below the higher limit of atmospheric oxygen (5 PPM) used in our setup. Here, we found that the fraction of cells exhibiting at least one fluorescent GFP foci after 2 h of treatment depends on antibiotic class and concentration, and varies in a dose-dependent manner (Figure 3D). As expected from the primary binding target, higher (0.1 μg/mL) doses of ciprofloxacin induced the largest increase in the fraction of positive cells, and nearly all cells exhibited DNA damage; additionally, increases of ~10 to 40% in the fraction of positive cells were found in cells treated with kanamycin and high concentrations of mecillinam (50× MIC; 10 μg/mL). Low doses of mecillinam, near the respective MIC, did not induce substantially higher levels of DNA damage compared to non-treatment on the timescale of our assay.

We next treated *E. coli* MG1655 with antibiotics in the presence of SYTOX Blue under anaerobic conditions (Figure 3E and Figure 3F). SYTOX Blue is a nucleic acid stain that only penetrates cells with damaged membranes, and is therefore a specific marker of membrane damage. Here, cells with compromised membranes are indicated by a largely uniform increase in fluorescence in the cellular cytoplasm. Similar to GamGFP cells, the fractions of positive cells after 4 h of treatment were increased in a dose-dependent manner for all three antibiotics (kanamycin, ciprofloxacin, mecillinam). Altogether, for treatment with all three antibiotics, the fractions of DNA damage- and membrane damage-positive cells were associated with relative levels of RES accumulation (Figure 3A and Figure 3B), with the exception of high concentrations of ciprofloxacin, for which we measured lower levels of RES but for which more cells exhibited DNA and membrane damage. While this may be expected for DNA damage due to ciprofloxacin's primary binding targets, the observation for membrane damage suggests that ciprofloxacin-treated cells may be more susceptible to membrane damage in a manner that is not directly proportional to RES accumulation.

The foregoing results suggest that, under anaerobic conditions, antibiotics induce DNA damage different from the damage directly induced by primary target binding for treatment with kanamycin and mecillinam, and membrane damage different from the damage directly induced by primary target binding for treatment with ciprofloxacin. It is important to note that our findings suggest that DNA damage is associated with—and may not necessarily be a cause of—antibiotic lethality. Yet, DNA damage could induce the SOS response, which may result in membrane alterations through the activities of repair proteins such as RecA (Garvey et al. 1985).

Additionally, these forms of damage may be also consistent with the antibiotic-induced accumulation of RES and other RMBs. Indeed, 4-HNE and MGO participate in a variety of cellular reactions, including reactions with DNA to form adducts and generation of additional free radicals that may result in lipid peroxidation (Note S1). Treating antibiotic-free cells exogenously with RES, we found that both 4-HNE and MGO induced DNA double-strand breaks and membrane damage in a dose-dependent manner and resulted in a wide range of fractions of GamGFP- or SYTOX Blue-positive cells, from 20% to 90%, that are similar to the fractions of positive antibiotic-treated cells at high concentrations (Figure S4). These findings indicate that the generation of 4-HNE and MGO in antibiotic-treated cells may contribute in part to the DNA or membrane damage induced by antibiotic treatment. Importantly, we note that not all antibiotic-treated cells are GamGFP- or SYTOX Blue-positive, suggesting that additional forms of cellular damage may be needed to fully explain antibiotic lethality.

Chemical scavengers of reactive metabolic byproducts decrease antibiotic lethality under anaerobic conditions

As RMBs are produced in cells treated with antibiotics under anaerobic conditions and RMBs, particularly RES, induce macromolecular damage consistent with that induced by antibiotics, we asked whether RMBs might contribute to antibiotic lethality. To address this question, we tested whether perturbations that rescue cells from RMBs also rescue cells from antibiotics under anaerobic conditions. Previous work has shown that thiourea, a general scavenger of RMBs, quenches RMB-sensitive fluorescent dye oxidation and protects against antibiotic killing both anaerobically (Keren et al. 2013; Liu et al. 2013) and aerobically (Kohanski et al. 2007), consistent with our finding of RMB accumulation under anaerobic conditions and the suggestion that thiourea may scavenge RMBs under different oxygen conditions. Contrasting arguments have posited that thiourea acts independently of scavenging RMBs and rescues cells by reducing growth or metabolic rate (Liu et al. 2013). Here, we demonstrate that protection against antibiotic lethality is general across different RMB scavengers and show that these scavengers typically reduce RES accumulation. We considered a panel of three chemical scavengers—glutathione, acetylcysteine, and pyridoxamine—which are known to detoxify various RMBs (Figure 4A and Note S2), and probed their effects on antibiotic killing under anaerobic conditions. Prior studies indicate that the nonenzymatic reactivity of glutathione or

acetylcysteine with H_2O_2 is limited (Imlay, 2015; Winterbourn et al. 1999; Zhitkovich, 2019), suggesting that their scavenging activities may predominantly target RES or RNS. Second-order rate constants have been measured to be ~0.1 to 1 M^{-1} s^{-1} for the nonenzymatic reaction of glutathione or acetylcysteine with H_2O_2 (Winterbourn et al. 1999; Deponte 2017), ~1 to 10 M^{-1} s^{-1} for glutathione with a variety of electrophiles (Chan et al. 2008), and ~10^9 M^{-1} s^{-1} for glutathione with nitric oxide (Deponte 2017). Thus, application of these scavengers may support the general involvement of RMBs in antibiotic lethality, rather than the specific contribution of H_2O_2 and ROS alone, as previously suggested (Imlay 2015).

We first focused on glutathione, which has been shown to increase the MICs of kanamycin and ciprofloxacin and attenuate antibiotic lethality under aerobic conditions (Wong et al. 2021a; Lopatkin et al. 2019) (Figure S1). To test whether these observations hold under anaerobic conditions, we performed MIC and time-kill assays with exogenous supplementation of glutathione at a concentration of 10 mM, identical to that used in previous aerobic measurements (Wong et al. 2021a). We found that exogenous addition of glutathione resulted in a 2-fold increase in the anaerobic kanamycin MIC, an 8-fold increase in the anaerobic ciprofloxacin MIC, and no increase in the anaerobic mecillinam MIC (Table S1), indicating that glutathione can confer protection—as indicated by increases in MIC—to kanamycin- and ciprofloxacin-treated cells. Substantial (>2-fold) increases in MIC were specific to ciprofloxacin, as limited MIC changes were observed in cells treated with the bacteriostatic antibiotics rifampicin, chloramphenicol, and tetracycline (Table S1). Additionally, consistent with these MIC values, CFU quantitation revealed decreased antibiotic killing of cells in the presence of glutathione (Figure 4B and Figure S6). After 4 h of treatment, anaerobic killing by kanamycin and ciprofloxacin was reduced by as much as 5 logs, and anaerobic killing by mecillinam was reduced by ~1 to 2 logs across a range of antibiotic concentrations (Figure 4B and Figure S6). Aside from unsubstantial killing (≤1 log of decreased survival) observed during mecillinam treatment under aerobic conditions, the observed anaerobic protection from antibiotic killing was largely similar to that under aerobic conditions (Figure 4B, Figure S1, and Figure S6). Moreover, while differences in MIC contribute to decreased lethality for kanamycin and ciprofloxacin, the observed increases in MICs were typically smaller than the shifts in concentration shown in the time-kill plots (Figure 4B and Table S1). This observation suggests that glutathione protects cells from kanamycin and ciprofloxacin killing only in part by increasing the MICs. In kanamycin-

and ciprofloxacin-treated cells, glutathione protection was reflected at the single-cell level, where the frequency of cytoplasmic condensation was decreased (Figure S2). The frequency of membrane bulging in mecillinam-treated cells was not significantly changed by glutathione supplementation, suggesting that, in mecillinam-treated cells, glutathione protection occurs independently from membrane bulging. We also found that glutathione decreases antibiotic lethality irrespective of the availability of environmental oxygen and the known effects of glutathione on cellular efflux and detoxification processes (Note S3, Figures S7-S10, and Tables S2-S4).

We next considered two other chemical scavengers of RMBs, acetylcysteine and pyridoxamine (Figure 4A and Note S2). Acetylcysteine, a glutathione precursor, is believed to be a poor scavenger of ROS but a potent scavenger of RES, with which it forms less-reactive Michael adducts (Zhitkovich, 2019; Negre-Salvayre et al. 2008), and can also serve as a precursor to H_2S (Shatalin et al. 2011; Mironov et al. 2017), whose anionic form (HS^-) reacts with RES via direct sulfhydration (Nishida et al. 2012). Pyridoxamine is known to primarily scavenge RES and prevent the formation of other toxic species including AGE and ALE, and may additionally scavenge ROS (Negre-Salvayre et al. 2008; Voziyan et al. 2005; Amarnath et al. 2004). We found that acetylcysteine and pyridoxamine, at concentrations (10 mM) comparable to glutathione supplementation, increased the anaerobic kanamycin and ciprofloxacin MICs similarly to glutathione, by 2- and 8-fold respectively, and did not affect the mecillinam MIC (Table S1). Additionally, and consistent with these MIC values, we found that exogenous supplementation of acetylcysteine and pyridoxamine attenuated antibiotic killing both anaerobically and aerobically (Figure 4B, Figure S1, and Figure S6). Similar to the observed protection against antibiotics for glutathione, we found that, at the single-cell level, supplementation of acetylcysteine and pyridoxamine reduced the frequency of cytoplasmic condensation in kanamycin- and ciprofloxacin-treated cells, but not the frequency of membrane bulging in mecillinam-treated cells (Figure S2).

Scavenger protection is not explained by alterations to metabolism, proton motive force, or intracellular antibiotic concentration under anaerobic conditions

As differences in cellular growth, metabolism, and intracellular concentration of antibiotics may affect antibiotic lethality, we performed additional experiments to determine whether these

factors could contribute to scavenger-mediated protection. Supplementation of each scavenger did not lead to significant differences in growth rate, as measured by optical density (Figure 4C). Previous studies from our laboratory and others (Lopatkin et al. 2019; Mathieu et al. 2016) have suggested that, under aerobic conditions, antibiotic lethality depends on the cellular metabolic state associated with ambient growth conditions, and that antibiotic lethality correlates with increased ATP levels (Lopatkin et al. 2019). As the BacTiter Glo assay has been used to measure ATP levels of bulk cultures (Lopatkin et al. 2019), we utilized this assay to determine ATP levels in scavenger-treated bulk cultures under anaerobic conditions. If decreased antibiotic lethality in the presence of scavengers (10 mM) arose due to decreased metabolism, then the measured ATP levels should be decreased in the presence of RMB scavengers. We found, on the contrary, that measured ATP levels were *increased* in the presence of RMB scavengers (Figure 4D and Figure S11). These findings are inconsistent with the hypothesis that scavenger protection from antibiotic lethality arises from suppressive alterations to bacterial metabolic state. Importantly, time-kill experiments with cells cultured and treated in diluted LB (1:1000 in PBS) confirm that decreasing metabolism alone is insufficient to explain the protection observed: we find that there is essentially no growth, and between 0 to 2 logs of killing, occurring in antibiotic-treated cells in dilute LB across all antibiotic concentrations tested (Figure S12 and Figure S13). In contrast, growth persists at lower antibiotic concentrations relative to the MICs in the presence of glutathione, acetylcysteine, or pyridoxamine in nutrient-replete media (Figure 4B). Together, these findings indicate that suppressive alterations to bacterial metabolic state do not explain the observed scavenger protection from antibiotic lethality.

A prior study (Ezraty et al. 2013) has linked iron chelator-mediated protection against aminoglycosides, ostensibly evidence for ROS-dependent aminoglycoside lethality (Kohanski et al. 2007), to changes in iron-sulfur clusters and electron transport chains resulting in altered proton motive force (PMF) and decreased aminoglycoside uptake. In *E. coli*, the PMF is generated by two components, the membrane potential, $\Delta\Psi$, and the pH gradient, ΔpH, across the membrane. We assayed for changes in $\Delta\Psi$ and ΔpH using two fluorescent dyes, $DiBAC_4(3)$ and ACMA, as well as for changes in membrane permeability using $DiSC_3(5)$, in the presence and absence of RMB scavengers. $DiBAC_4(3)$ can enter depolarized cells, where it binds to intracellular proteins or the cell membrane and exhibits enhanced green fluorescence. ACMA is a DNA intercalator that selectively binds to poly (d(A-T)) and membranes in the energized state,

and becomes quenched if a pH gradient forms. $DiSC_3(5)$ accumulates on hyperpolarized membranes and can be translocated into the lipid bilayer. We found that the fluorescence intensities of $DiBAC_4(3)$-, ACMA-, and $DiSC_3(5)$-labeled cells, measured at the single-cell level, were not significantly different in the presence of RMB scavengers (Figure 4E). In contrast, as controls for these dyes, we used CCCP, a PMF decoupling protonophore, and valinomycin, an ionophore antibiotic. Consistent with the suppression of PMF in positive controls, we found that CCCP induced fluorescence of $DiBAC_4(3)$ and quenching of ACMA (Figure 4E). Consistent with changes in membrane permeability induced by valinomycin, we found that $DiSC_3(5)$-labeled cells fluoresced in the presence of valinomycin (Figure 4E). These findings suggest that the observed scavenger protection from antibiotic lethality does not arise from suppressive alterations to PMF.

Lastly, we performed intracellular antibiotic concentration measurements using fluorimetry for kanamycin and liquid chromatography-mass spectrometry (LC-MS) for ciprofloxacin and mecillinam. We treated cells with antibiotics at a constant concentration in the presence of scavenger (10 mM), and found approximately equal antibiotic concentrations in cells with and without scavenger, as indicated by single-cell measurements for cells treated with a fluorescent derivative of kanamycin and LC-MS measurements for bulk-culture ciprofloxacin- and mecillinam-treated cell lysates (Figure 4F). These results indicate that intracellular antibiotic concentrations are not decreased in any of the scavenger-antibiotic pairs. Altogether, these findings suggest that the observed scavenger-mediated increases in MICs and protection from antibiotic killing are not explained by differences in cellular growth rate, cellular metabolic state, PMF, or intracellular antibiotic concentration.

Scavenger protection is associated with decreased accumulation of reactive electrophilic species and reduced macromolecular damage under anaerobic conditions

To test the hypothesis that RMB scavengers protect cells from antibiotic action in part by scavenging RES, we directly measured the effects of scavenger supplementation on RES levels using GC-MS. We treated cells with antibiotics at approximately the same multiples of their corresponding MIC values in the presence and absence of glutathione, acetylcysteine, or pyridoxamine (10 mM) in order to account for MIC changes induced by scavengers (Table S1). In cells treated with similar concentrations of antibiotics relative to multiples of the respective

MICs, we found that 4-HNE and MGO concentrations after 2 h of treatment were largely decreased in the presence of scavengers (Figure 5A). The only exception was for kanamycin-treated cells in the presence of glutathione, which exhibited average MGO values larger than those of kanamycin-treated cells without scavenger. Notably, RES levels were decreased >2-fold under nearly all conditions with acetylcysteine and pyridoxamine, and similar decreases were observed for the application of scavengers to positive controls, in which cells were treated with exogenous MGO (Figure S14). Additionally, we found that these decreases in RES were often associated with decreases in DNA and/or membrane damage (Figure 5B) and reflected decreases in antibiotic lethality (Figure 5C). Indeed, scavengers also mitigated DNA and membrane damage induced by exogenous RES, and rescued cells from RES lethality when RES were administered exogenously (Figures S14-S16). We note that these scavenger-mediated decreases in RES levels—along with cellular responses such as filamentation and the induction of the SOS response—may, in addition to decreasing antibiotic lethality (Figure 4C), also contribute to the observed increases in antibiotic MICs (Table S1). Together, these findings support the hypothesis that glutathione, acetylcysteine, and pyridoxamine decrease antibiotic lethality in part by reducing RES levels. As antibiotics are still lethal to scavenger-treated cells for which reduced RES levels were measured after 2 h of treatment, our findings further highlight the possibilities that substantial increases in RMB levels may occur post-plating (Hong et al. 2019) and that, in addition to RES, other RMBs or cellular pathways affected by primary target-binding may also contribute to antibiotic lethality.

DISCUSSION

Understanding how bactericidal antibiotics kill bacteria remains an unresolved problem. In particular, while the field has classified primary antibiotic binding targets, how such binding leads to bacterial cell death remains unclear. We have previously proposed that, downstream of primary target binding, the induction of stress response pathways in response to corrupted cellular processes leads to energetic demands that heighten metabolic activity (Kohanski et al. 2007; Dwyer et al. 2007; Lobritz et al. 2015; Stokes et al. 2019). Increased metabolism results in the accumulation of RMBs, which promiscuously react with, and damage, cellular macromolecules, contributing to antibiotic lethality. This hypothesis was initially supported by our observations that treatment with bactericidal, but not bacteriostatic, antibiotics under aerobic

conditions increased hydroxyl radical formation via the Fenton reaction, that the iron chelator 2,2'-dipyridyl and the hydroxyl radical scavenger thiourea reduce antibiotic lethality, and that genetic perturbations to metabolic pathways—for instance, deletion of the *E. coli iscS* gene, which decreases iron-sulfur cluster abundance—affect antibiotic lethality (Kohanski et al. 2007). Subsequent studies, from multiple laboratories using independent lines of evidence (Gusarov et al. 2009; Wang et al. 2009; Davies et al. 2009; Yeom et al. 2010; Shatalin et al. 2011; Nguyen et al. 2011; Luo et al. 2012; Dwyer et al. 2012; Grant et al. 2012; Brynildsen et al. 2013; Moronez-Ramirez et al. 2013; Hong et al. 2019; Drlica et al. 2020), have supported this hypothesis. Downstream of treatment with bactericidal antibiotics, these studies have measured increases in energetic demands, cellular respiration rate, and cellular metabolism (Lobritz et al. 2015; Dwyer et al. 2014; Mathieu et al. 2016; Yang et al. 2019); investigated associated processes such as the stringent response, which activates when protein synthesis is increased and amino acid pools are depleted, and in turn increases ROS production (Nguyen et al. 2011; Khakimova et al. 2013; Mathieu et al. 2016); studied redox-related alterations to bacterial cell physiology (Dwyer et al. 2007; Belenky et al. 2015; Dwyer et al. 2012; Hong et al. 2019; Wang et al. 2009; Dwyer et al. 2014; Wong et al. 2021a) and cellular mutagenesis (Kohanski et al. 2010b; Gutierrez et al. 2013; Pribis et al. 2019); and demonstrated that RMBs—including ROS—and related metabolism-associated changes impact antibiotic lethality (Brynildsen et al. 2013; Hong et al. 2019; Gusarov et al. 2009; Dwyer et al. 2014; Wong et al. 2021a; Lopatkin et al. 2019; Goswami et al. 2016; Giroux et al. 2017). This common mechanism, as a working hypothesis for how bactericidal antibiotics, in part, kill bacteria has generated testable predictions and motivated potential strategies and targets for antimicrobial therapies.

In the present study, we have shown that bactericidal antibiotic treatment of *E. coli* under anaerobic conditions is associated with the accumulation of central carbon metabolites (Figure 1) and phenotypic changes (Wong et al. 2021a) that also occur under aerobic conditions (Figure 2), and that various RMB-sensitive dyes, including those sensitive to lipid peroxidation, RNS, and ROS, fluoresce in antibiotic-treated cells (Figure 2). Our observations of cytoplasmic condensation—indicative of membrane damage and cell death (Wong et al. 2021a)—and lipid peroxidation in antibiotic-treated cells suggest that RMBs might directly react with membrane lipids, producing promiscuous RES. Using GC-MS, we measured endogenous concentrations of two RES, 4-HNE and MGO, in antibiotic-treated cells and found that they are present under

anaerobic conditions (Figure 3). We also showed that antibiotic treatment under anaerobic conditions induces DNA double-strand breaks and membrane damage, consistent with possible contributions of RES damage to these macromolecules (Figure 3). Further work should address whether these or other forms of associated macromolecular damage are direct causes of antibiotic lethality. Importantly, three diverse RMB scavengers—glutathione, acetylcysteine, and pyridoxamine—reduce antibiotic lethality without decreasing cellular growth rate, cellular ATP levels, PMF, and intracellular antibiotic concentration (Figure 4). Instead, consistent with the proposed contribution of RMBs to cellular death, application of these scavengers generally decreased RES levels (Figure 5) and, for certain treatments, alleviated DNA and/or membrane damage (Figure 5) under anaerobic conditions.

Based on these results, we propose that RMBs, particularly RES, contribute to antibiotic-induced cell death in the absence of environmental oxygen according to the following mechanism (Figure 6). Upon binding of the primary drug target, antibiotics corrupt target-specific cellular processes, leading to increases in energetic demands and metabolic fluxes. RMBs, including but not limited to RES, RNS, and ROS, are generated by increased metabolic flux through anaerobic energy-generating processes and additional processes such as free radical interactions under anaerobic conditions. These RMBs promiscuously react with, and damage, cellular components including nucleic acids, proteins, and lipids, contributing in part to antibiotic lethality.

The hypothesis that RMBs contribute to antibiotic-induced bacterial cell death has been a model that has evolved and expanded, and should continue to be tested by additional experiments and analyses. Considerable evidence, from both the present study and others, are consistent with a contribution of RMBs, including RES, RNS, and ROS, to antibiotic-induced cell death under anaerobic and aerobic conditions (Kohanski et al. 2007; Dwyer et al. 2007; Gusarov et al. 2009; Wang et al. 2009; Davies et al. 2009; Girgis et al. 2009; Yeom et al. 2010; Shatalin et al. 2011; Nguyen et al. 2011; Foti et al. 2012; Luo et al. 2012; Dwyer et al. 2012; Grant et al. 2012; Brynildsen et al. 2013; Moronez-Ramirez et al. 2013; Dwyer et al. 2014; Lobritz et al. 2015; Belenky et al. 2015; Goswami et al. 2016; Takahashi et al. 2017; Hong et al. 2019; Stokes et al. 2019; Drlica et al. 2020; Wong et al. 2021a; Lopatkin et al. 2021). Bacterial cell death is a biologically complex process, and we may expect that additional RMBs and

pathways contributing to antibiotic-induced cell death remain to be uncovered, understood, and exploited by our evolving understanding of how antibiotics work.

Limitations of the study

In this work, we have combined single-cell and bulk culture approaches to study the metabolic and molecular pathways contributing to antibiotic-induced cell death in *E. coli*. Building on previous studies (Kohanski et al. 2007; Dwyer et al. 2007; Dwyer et al. 2014; Lobritz et al. 2015; Wong et al. 2021a), we have focused on *E. coli* as a well-studied model organism. Our findings suggest that RMBs contribute to antibiotic lethality under anaerobic conditions. This suggestion applies to different strains of *E. coli*, as shown here, and RMB scavengers protect against gentamicin lethality as well for a multidrug-resistant clinical *E. coli* isolate (Figure S17). However, the extent to which similar findings generalize to other bacteria—which may thrive under various oxygen conditions—and antibacterial treatments will require further study. Additionally, as detailed further in *STAR Methods*, our experimental setup limits the concentration of O_2 in our experiments to below ~30 μM using a hydrogen in nitrogen gas mix. Although similar experimental setups have been used to study the effects of environmental oxygen on antibiotic lethality (Keren et al. 2013; Liu et al. 2013; Dwyer et al. 2014; Wong et al. 2021a), we note that micromolar concentrations of O_2 have been shown to accommodate terminal oxidase function, and ROS formation, in plants (Blokhina et al. 2001). Furthermore, hydrogen gas may possess antioxidant properties, which could alter RMB generation and its downstream deleterious effects (Ohsawa et al. 2007). These limitations are consistent with our hypothesis that RMBs may arise from trace amounts of molecular oxygen, in addition to various endogenous sources including anaerobic respiration with alternate terminal electron acceptors and free radical interactions. We expect future work to further address these limitations, for instance using anaerobic environments containing noble gases such as argon.

Acknowledgements

We thank the past and present members of the Collins lab for helpful discussions. We thank Susan M. Rosenberg for generously providing the GamGFP strain of *E. coli* used in this study. F.W. was supported by the James S. McDonnell Foundation. J.M.S. was supported by the Banting Fellowships Program (393360). S.C.B. was supported by a National Science Foundation Graduate Research Fellowship (112237). J.J.C. was supported by the Defense Threat Reduction Agency (grant number HDTRA1-15-1-0051), the National Institutes of Health (grant number R01-AI146194), and the Broad Institute of MIT and Harvard.

Author contributions

F.W. and J.J.C. conceived the project. F.W. and J.M.S. designed experiments. F.W. performed experiments. S.C.B. assisted with strain construction. C.V. and S.A.T. performed GC-MS and LC-MS experiments. All authors contributed to data interpretation and analysis. F.W. and J.J.C. wrote the manuscript with the assistance of all authors. F.W. and J.J.C. supervised the project.

Declaration of interests

J.J.C. is scientific co-founder and scientific advisory board chair of EnBiotix, an antibiotic drug discovery company, and PhareBio, a non-profit venture focused on antibiotic drug development. J.M.S. is scientific co-founder and scientific director of PhareBio. The remaining authors declare no competing interests.

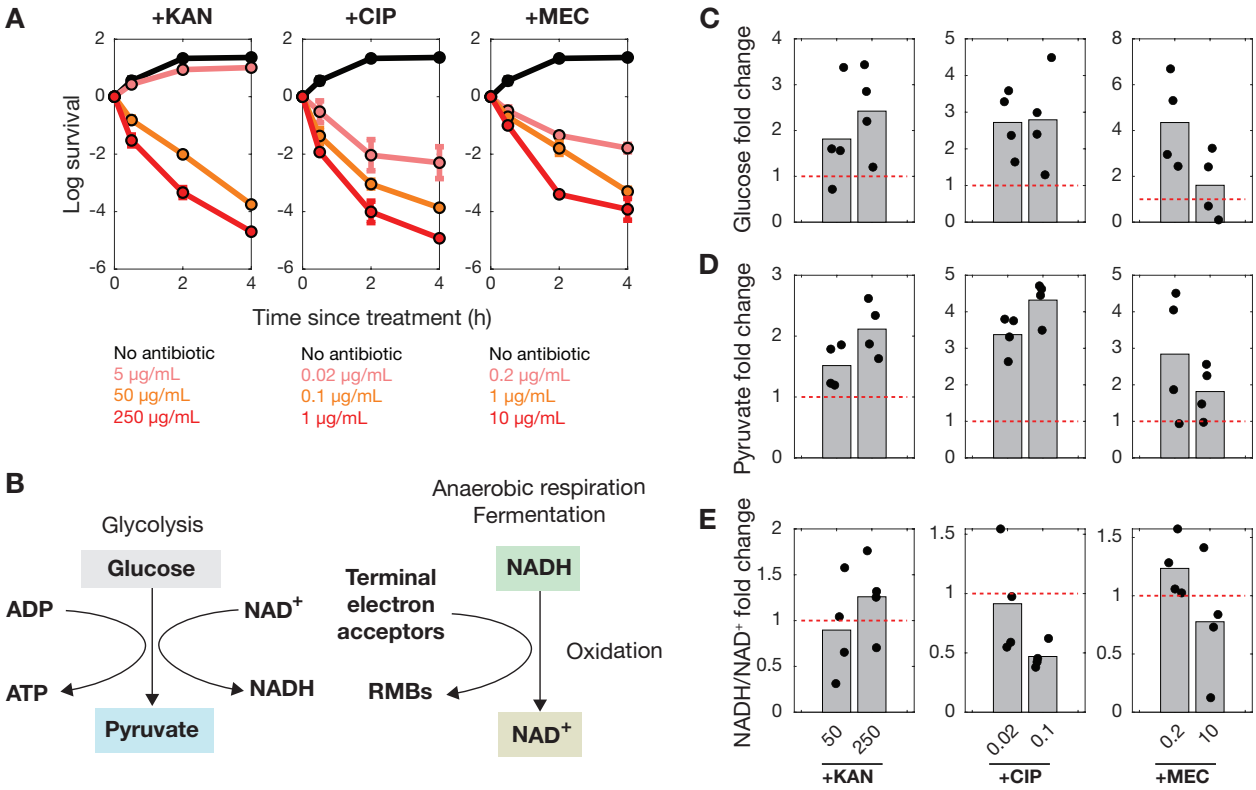

590

591 **Figure 1. Antibiotic treatment results in decreased survival and changes to glucose,**
592 **pyruvate, and NADH/NAD$^+$ concentrations under anaerobic conditions.**

593 (A) Survival curves of log-phase *E. coli* bulk cultures treated with kanamycin (KAN),
594 ciprofloxacin (CIP), and mecillinam (MEC) at various concentrations, corresponding to 0.1× to
595 50× the anaerobic MICs (Table S1), as determined by plating and CFU quantitation. In
596 particular, the anaerobic MICs for kanamycin, ciprofloxacin, and mecillinam were taken as 50
597 μg/mL, 0.02 μg/mL, and 0.2 μg/mL, respectively. Here and below, *E. coli* MG1655 was used
598 unless otherwise indicated. Cells were cultured, treated, and plated in LB under anaerobic
599 conditions. Error bars indicate one standard deviation, and each curve is representative of two
600 biological replicates. Data are presented as mean values +/- SEM; where SEM is small, error
601 bars are present but are inside symbols.

602 (B) A schematic illustrating the roles of glucose, pyruvate, and NADH/NAD$^+$ in *E. coli*
603 glycolysis and anaerobic respiration.

604 (C-E) Bulk-culture fold change in glucose concentration (C), pyruvate concentration (D), and
605 NADH/NAD$^+$ concentration (E) following treatment with various concentrations of kanamycin,
606 ciprofloxacin, and mecillinam under anaerobic conditions. Metabolite concentration values are
607 normalized by corresponding protein concentrations, then divided by the average of at least four
608 untreated measurements to calculate fold change relative to untreated controls. Antibiotic-treated
609 cells were cultured in LB, then harvested after 20 min of treatment with antibiotics at the
610 concentrations (μg/mL) shown. Bars indicate mean values, and data show four biological
611 replicates (black points). Red dashed lines indicate a fold change of 1, corresponding to
612 measurements for untreated cells.

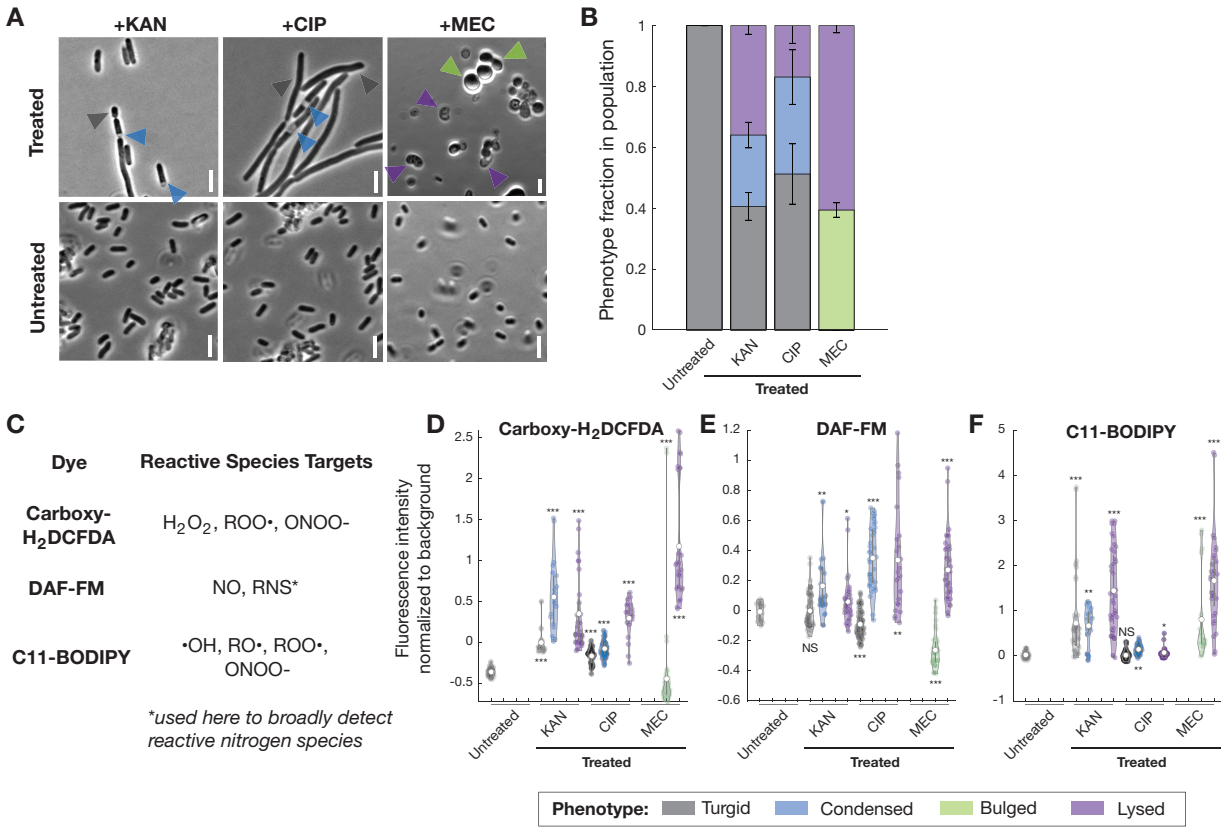

Figure 2. Phenotypic change and fluorescence of reactive metabolic byproduct-sensitive dyes occur under anaerobic conditions.

(A) Cellular phenotypic changes induced by antibiotic treatment, at bactericidal concentrations corresponding to 1× to 50× the anaerobic MICs (Table S1). Concentrations used were as follows: kanamycin 50 μg/mL; ciprofloxacin, 1 μg/mL; mecillinam, 10 μg/mL. Images are shown in phase contrast, and colored arrows highlight specific phenotypes (bottom of figure). Cells were imaged 4 h after antibiotic treatment, and images are representative of three different fields of view from two biological replicates. Scale bars, 3 μm.

(B) Census of single-cell phenotypes in populations treated with antibiotics at the concentrations indicated in (A) after 4 h. Data are from four fields of view from four biological replicates with at least 150 cells per group. Colors refer to the legend at the bottom of the figure. Data are presented as mean values +/- SEM, and error bars indicate one standard deviation.

(C) Summary of a panel of RMB-sensitive dyes and their primary reactive species targets.

(D-F) Fluorescence intensities of RMB-sensitive dyes in single cells, after treatment at the concentrations indicated in (A), which exhibit different post-treatment phenotypes, as determined by epifluorescence microscopy after 4 h of treatment. Values indicate fluorescence intensities relative to background levels. Cells were cultured, treated, and imaged under anaerobic conditions. White points indicate mean values, and each distribution is representative of at least 10 cells. Two-sample Kolmogorov-Smirnov tests for differences from untreated, turgid cells: NS, not significant, $*p < 10^{-2}$, $**p < 10^{-4}$, $***p < 10^{-10}$. Columns with no data, indicating that the specified phenotypes were not observed, are not shown.

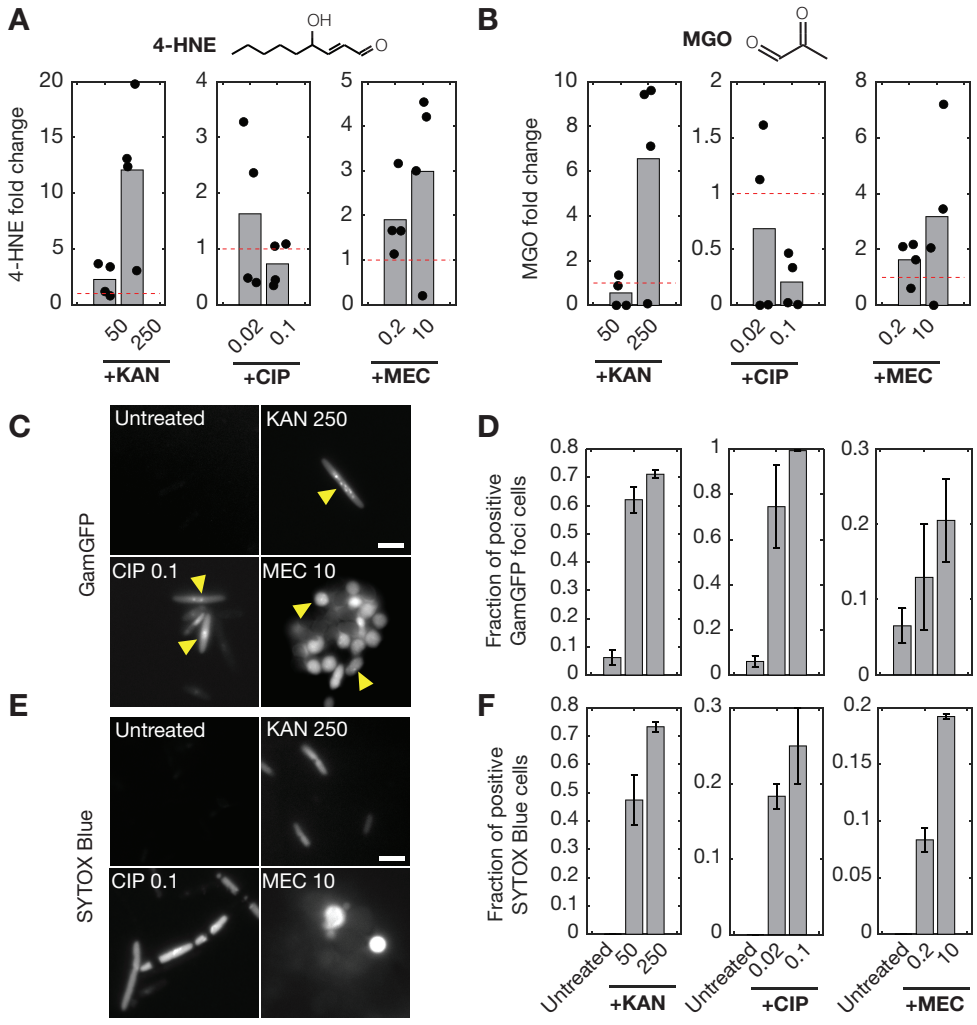

Figure 3. Antibiotic-treated cells accumulate reactive electrophilic species and display dose-dependent macromolecular damage under anaerobic conditions.

(A-B) GC-MS measurements of 4-HNE and MGO concentration fold changes relative to non-treatment in cell lysates. RES concentration values are normalized by corresponding protein concentrations, then divided by the average of at least four untreated measurements to calculate fold change relative to untreated controls. Antibiotic-treated cells were cultured in LB, then harvested after 2 h of treatment with antibiotics at the concentrations (μg/mL) shown. Bars indicate mean values, and data show four biological replicates (black points). (Top) Chemical structures of 4-HNE and MGO.

(C-D) Fluorescence microscopy images and quantification of GamGFP loci in antibiotic-treated cells (*E. coli* strain SMR14334). Cells were treated with antibiotics at the indicated concentrations (μg/mL) under anaerobic conditions, then imaged after 2 h of treatment. Yellow arrows in (C) highlight GFP foci indicating DNA double-strand breaks. Error bars in (D) represent the full range of fractional values observed in at least two independent fields of view from two biological replicates, and each bar is representative of at least 10 cells. Scale bar, 3 μm.

(E-F) Similar to (C,D), but for *E. coli* MG1655 fluorescently labeled with SYTOX Blue, a membrane damage-sensitive dye, imaged after 4 h of treatment.

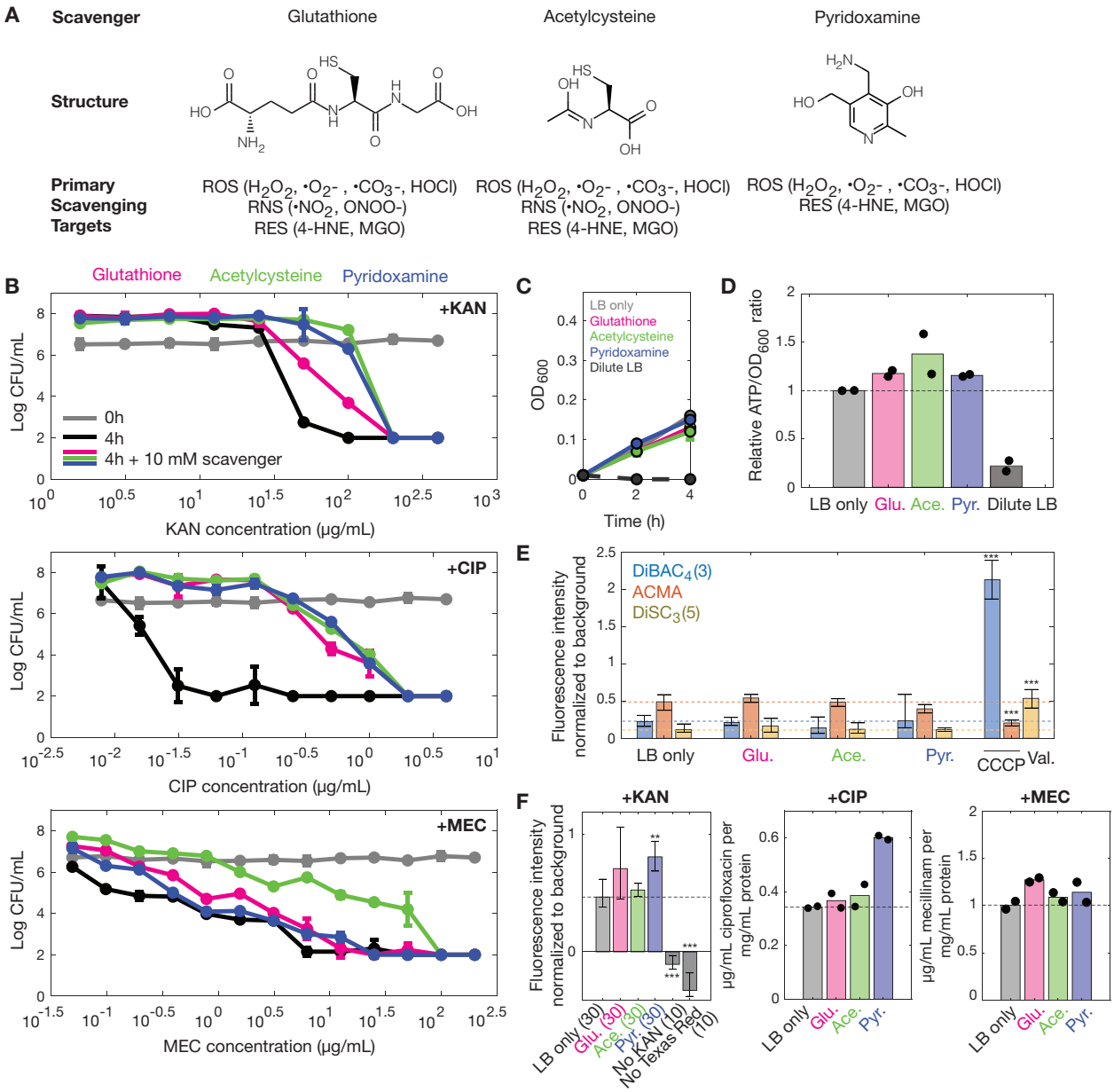

Figure 4. Reactive metabolic byproduct scavengers protect against antibiotic lethality under anaerobic conditions, which is not explained by alterations to cellular growth rate, cellular metabolism, proton motive force, and intracellular antibiotic concentration.

(A) RMB scavengers and their primary scavenging targets. Examples of reactive species targets are indicated in parentheses.

(B) Survival curves of *E. coli* MG1655 after kanamycin, ciprofloxacin, and mecillinam treatment at various concentrations, with and without exogenous supplementation of RMB scavengers (10 mM), as determined by plating and CFU counting. Cells were cultured, treated, and plated in LB under anaerobic conditions. Error bars indicate one standard deviation, and each point is representative of two biological replicates. Data are presented as mean values +/- SEM; where SEM is small, error bars are present but are inside symbols. Where applicable, CFU/mL values

less than 10^2 were truncated to a value of 10^2 to reflect the lower limit of quantification.

(C) OD_{600} measurements for anaerobic cell cultures supplemented with RMB scavengers (10 mM) or grown in dilute LB. Error bars indicate one standard deviation, and data are presented as mean values +/- SEM. Where SEM is small, error bars are present but are inside symbols. Data from two biological replicates in each condition are shown.

(D) Ratios of ATP luminescence values to OD_{600} values, relative to cultures grown in LB without scavengers. Treated cells were grown, without antibiotics, anaerobically with RMB scavengers for 2 h, then harvested. Data from two biological replicates are shown (black points), and bars indicate average values.

(E) Single-cell measurements of $DiBAC_4(3)$, ACMA, and $DiSC_3(5)$ fluorescence, which respectively detect changes in the $\Delta\Psi$ and ΔpH components of PMF and changes in membrane permeability. Data from cells treated with 1 mM carbonyl cyanide m-chlorophenylhydrazone (CCCP), a PMF uncoupler, are shown as a positive control for $DiBAC_4(3)$ and ACMA, and data from cells treated with 100 μg/mL valinomycin, an ionophore, are shown as a positive control for $DiSC_3(5)$. Data are presented as mean values +/- SEM, and error bars indicate 95% confidence intervals for the mean. Data representative of 20 cells in each group. Two-sample *t*-tests for differences in mean values from LB only: $***p < 10^{-5}$, all other bars not significant.

(F) Intracellular antibiotic concentration measurements. Cells were treated with kanamycin-Texas Red (50 μg/mL), ciprofloxacin (1 μg/mL), or mecillinam (10 μg/mL) for 1 to 4 h under anaerobic conditions, and intracellular antibiotic concentrations were assayed fluorometrically (kanamycin) or using LC-MS (ciprofloxacin and mecillinam). Single-cell counts for kanamycin-treated cells are indicated in parentheses, and 95% confidence intervals for the mean are shown. Two-sample *t*-tests for differences in mean values of cells with no scavenger: $**p < 10^{-3}$, $***p < 10^{-5}$, all other bars not significant. For ciprofloxacin and mecillinam, data from two biological replicates in bulk culture are shown (black points), and bars indicate average values. Dashed lines indicate baseline values.

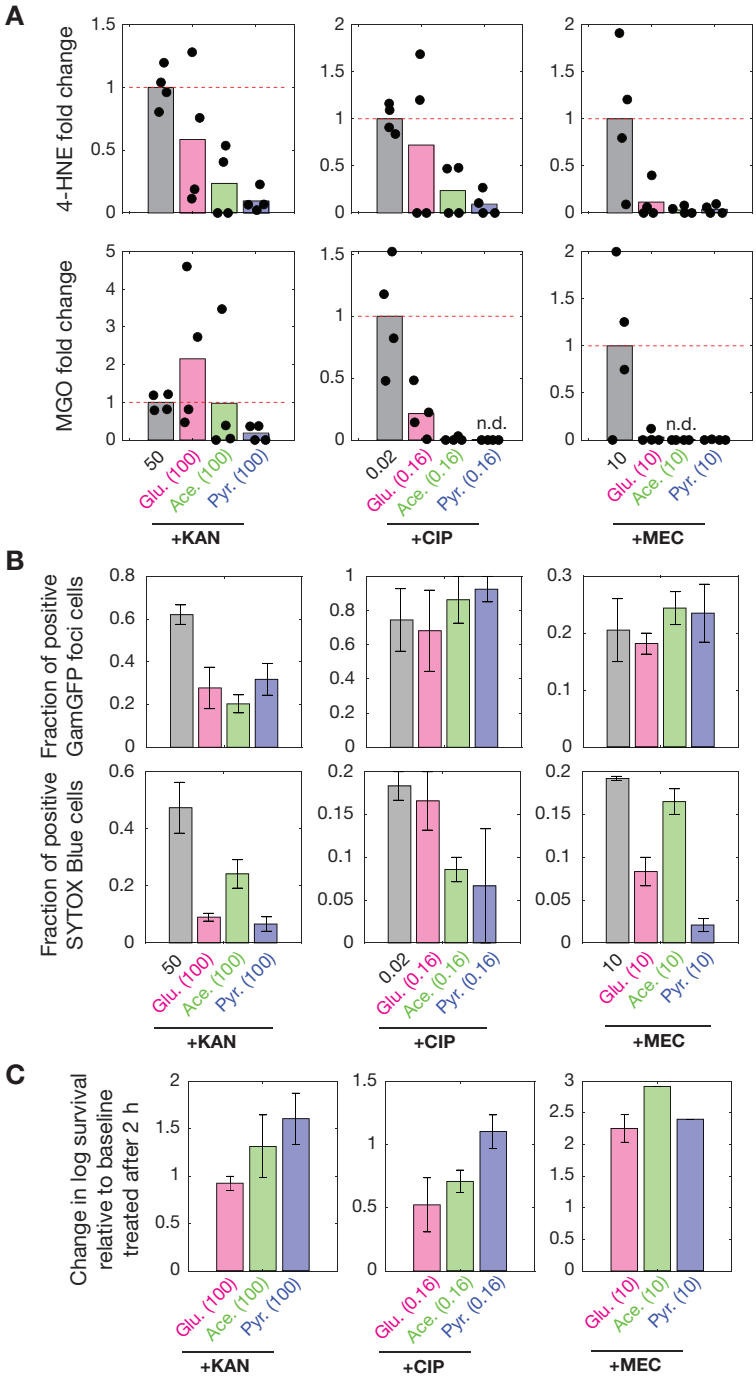

691

692 **Figure 5. Reactive metabolic byproduct scavengers reduce reactive electrophilic species**
693 **under anaerobic conditions.**

694 (A) GC-MS measurements of 4-HNE and MGO concentration fold changes relative to non-
695 treatment in cell lysates. RES concentration values are normalized by corresponding protein
696 concentrations, then divided by the average of at least four baseline treatment measurements to
697 calculate fold change relative to baseline treated cells. Antibiotic-treated cells were cultured in
698 LB, then harvested after 2 h of treatment with antibiotics at the concentrations (μg/mL) shown.
699 Cells were treated at concentrations corresponding to similar MIC multiples. Where applicable,

scavengers were exogenously supplemented at a concentration of 10 mM. Bars indicate mean values, and data show four biological replicates (black points); n.d., not detected in all replicates.

(B) Quantification of GamGFP loci and SYTOX Blue fluorescence in antibiotic-treated cells (*E. coli* strains SMR14334 and MG1655, respectively). Cells were treated with antibiotics at the indicated concentrations (μg/mL) under anaerobic conditions. Where applicable, scavengers were supplemented at a concentration of 10 mM. Cells were imaged after 2 h (GamGFP) or 4 h (SYTOX Blue) of treatment, and error bars represent the full range of fractional values observed in at least two independent fields of view from two biological replicates. Each bar is representative of at least 20 cells.

(C) Scavenger-induced changes in cellular survival after antibiotic treatment at the indicated concentrations (μg/mL) in the presence of scavengers (10 mM) under anaerobic conditions. Baseline values correspond to those after treatment with antibiotics at the baseline concentrations shown in (A,B). Measurements are based on CFU/mL counts after 2 h of treatment and are representative of two biological replicates. Error bars indicate one standard deviation.

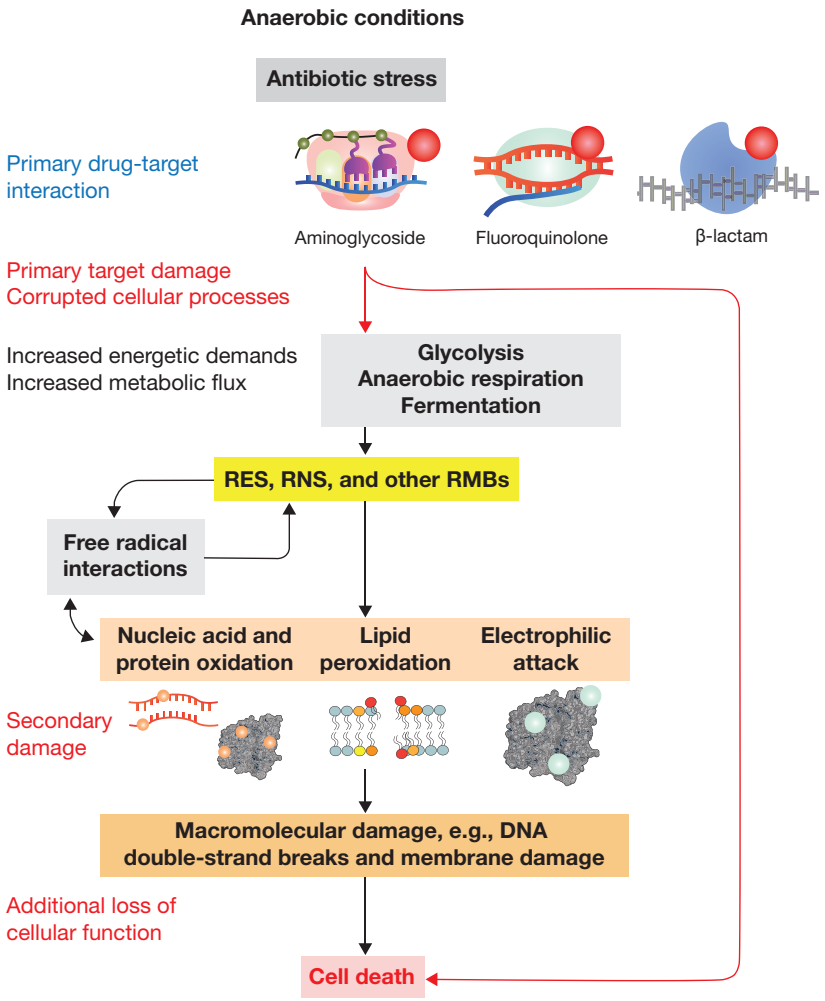

Figure 6. Proposed model of the contribution of RES and other RMBs to antibiotic lethality under anaerobic conditions.

Upon binding of the primary drug target, antibiotics induce target-specific corruption of cellular processes, leading to increased energetic demands and elevated metabolic flux. RMBs, including but not limited to RES and RNS, are generated by increased metabolic flux and additional processes such as free radical interactions. These RMBs lead to additional free radical interactions and promiscuously react with cellular components including nucleic acids, proteins, and lipids, resulting in macromolecular damage which contributes in part to antibiotic lethality.

STAR Methods

RESOURCE AVAILABILITY

Lead contact. Further information and request for resources and reagents should be directed to and will be fulfilled by the lead contact, James J. Collins (jimjc@mit.edu).

Materials availability. The strains of *E. coli* used in this study are available with a materials transfer agreement (MTA).

Data and code availability. Any additional information required to reanalyze the data reported in this paper is available from the lead contact upon request.

EXPERIMENTAL MODEL DETAILS

Bacterial strains. All experiments were performed with *E. coli* K-12 MG1655 unless otherwise noted, and all strains used in this work are summarized in Table S3. The Δ*kefB*Δ*kefC* double knockout strain was constructed from the Keio collection (Baba et al. 2006) Δ*kefB* and Δ*kefC* strains (Δ*kefB*, JW3313-1; Δ*kefC*, JW0046-1) by lambda-red recombineering and kanamycin resistance was subsequently cured, both according to published methods (Datsenko et al. 2000); a list of primers used in the construction and PCR verification is provided in Table S4. The Δ*gstA* single knockout strain is from the Keio collection (Δ*gstA*, JW1627-1) and was validated using PCR. For time-kill experiments involving the Δ*kefB*Δ*kefC* and Δ*gstA* strains, the Keio collection parent strain, *E. coli* BW25113, was used as the control strain. SMR14334, a GamGFP strain, is a derivative of strain MG1655 and has been previously described (Shee et al. 2013). *E. coli* CDC 541, a multidrug-resistant strain, was obtained from the Centers for Disease Control and Prevention AR Isolate Bank (Atlanta, GA).

METHOD DETAILS

Antibiotics. Kanamycin sulfate (product 60615, Sigma-Aldrich, St. Louis, MO) and gentamicin sulfate (Sigma-Aldrich G1914) were dissolved in ultrapure Milli-Q water to make working stock solutions of up to 25 mg/mL. Ciprofloxacin (Sigma-Aldrich 17850) was dissolved in dilute acid (0.1 M HCl, Sigma-Aldrich H1758) to make working stock solutions of up to 10 mg/mL. Mecillinam (Sigma-Aldrich 33447) was dissolved in dimethyl sulfoxide (DMSO, Sigma-Aldrich D5879) to make working stock solutions of up to 10 mg/mL. Rifampicin (Sigma-Aldrich R3501), chloramphenicol (Sigma-Aldrich C0378), and tetracycline (Sigma-Aldrich 87128) were dissolved in DMSO, ethanol, and dilute acid, respectively, to make working stock solutions of 3.2 mg/mL. All antibiotics were freshly prepared immediately before each experiment.

Bacterial culture and growth. Cells were grown in liquid LB medium (product 244620, Becton Dickinson, Franklin Lakes, NJ). LB media containing 1.5% agar (Becton Dickinson 244520) was used to grow individual colonies. Cells were grown anaerobically or aerobically from single colonies at 37°C in 14 mL Falcon tubes with shaking at 300 rpm.

In anaerobic experiments, as a redox indicator, resazurin (Sigma-Aldrich R7017) was added to LB to a final concentration of 1 mg/L before autoclaving; the heat-activated form of

resazurin, resorufin, is colorless below a redox potential of -110 mV (Reddy et al. 2007). We note that resorufin remained strictly colorless in all anaerobic time-kill experiments, with the exception of those with exogenous H_2O_2. Addition of H_2O_2 resulted in rapid and persistent color changes of resorufin to pink, indicating increases in redox potential.

Determination of MICs. We determined MICs anaerobically for all antibiotics and RES considered in this work against *E. coli* MG1655 by diluting 1:10,000 from an anaerobically-grown overnight culture into 96-well plates (product 9018, Corning Inc., Corning, NY) capped with plate lids, with no shaking and two-fold dilutions of antibiotic or RES across wells. The MIC was determined as the minimum concentration of antibiotic or RES at which no visible growth (optical density at 600 nm, $OD_{600} < 0.1$) occurred overnight while incubated anaerobically at 37°C. A summary of the MIC values determined in this way is provided in Tables S1 and S2. All OD_{600} measurements in this work were performed using between 100 and 200 µL of culture volume in 96-well plates with a SpectraMax M3 plate reader (Molecular Devices, San Jose, CA).

Anaerobic chamber and experiments. Experiments were performed in an anaerobic chamber (Type B Vinyl, Coy Labs, Grass Lake, MI) equipped with twin palladium catalysts and a Coy Oxygen/Hydrogen Analyzer (Coy Labs) and maintained at 37°C. A 5% hydrogen in nitrogen gas mix (product NI HY5300, AirGas, Radnor, PA) was used to maintain the steady-state anaerobic environment at less than 5 PPM oxygen. Additionally, a BD BBL GasPak anaerobic indicator (Becton Dickinson), and growth media containing 1 mg/L resorufin as an anaerobic indicator, were used to validate anaerobic conditions. The minimum sensitivity of the oxygen indicators used is ~1 PPM; hence the concentration of O_2 in the experiments was below ~30 µM. While previous studies have assumed that similarly anaerobic conditions were stringent enough to prevent ROS formation (Keren et al. 2013; Liu et al. 2013), we note here that, inconsistent with this assumption, micromolar concentrations of O_2 have been shown to accommodate terminal oxidase function, and ROS formation, in plants (Blokhina et al. 2001). These results are consistent with our hypothesis that RMBs can arise from trace amounts of molecular oxygen, in addition to various endogenous sources including anaerobic respiration with alternate terminal electron acceptors and free radical reactions.

For all anaerobic experiments, starting cultures were taken from cultures grown overnight inside the anaerobic chamber. Cells were grown with shaking at 300 rpm in 14 mL Falcon tubes and treated with antibiotics or RES as described above. For time-kill assays, cells were serially diluted, plated, and grown overnight inside the anaerobic chamber. For microscopy experiments, cells were plated and imaged with a Zeiss Axioscope A1 microscope inside the anaerobic chamber, as detailed further below. Plating and microscopy were performed strictly inside the anaerobic chamber.

To allow for deoxygenation, all materials used in our experiments were brought into the anaerobic chamber at least 24 h before the start of the experiment, with the exception of antibiotics or RES, fluorescent dyes and reagents, RMB scavengers, the BacTiter-Glo solution for ATP measurements, and cell lysis solution containing B-PER for preparation of cell lysates. To ensure freshness of these reagents, these reagents were prepared immediately before each experiment, brought into the anaerobic chamber, and equilibrated in open-cap tubes for 1 to 2 h before usage. After addition of these reagents to growing cultures, with the exception of ROS-treated cultures, we observed that resorufin in the growth media remained strictly colorless,

indicating that these reagents did not introduce significant sources of environmental oxygen to our experiments.

Time-kill assays and CFU measurements. For all time-kill assays in bulk culture, cells were diluted 1:100 from an overnight culture (grown either anaerobically or aerobically, corresponding to the oxygen conditions of the time-kill experiment) into 14 mL Falcon tubes containing 2 mL of growth media. Following previous work (Keren et al. 2013) in which cells were grown for a fixed incubation time under both anaerobic and aerobic conditions, here cells were grown for ~1.5 h to early exponential phase, $OD_{600} \approx 0.02$ (anaerobic) and 0.1 (aerobic), in the conditions described above; we note here that the starting densities between this work and previous work from our lab (Dwyer et al. 2014) differ, and this difference may contribute to differences in survival relative to previous work from our lab (Dwyer et al. 2014). Antibiotics were added to the final concentrations indicated, and cultures were re-incubated with shaking at 300 rpm at 37°C. At the indicated times, cells were aliquoted and serially diluted in LB, and between 5 to 100 μL of cell culture was plated or spotted on LB agar.

LB-agar petri dishes were incubated at 37°C at least overnight (16-24 h) under the same oxygen conditions as the time-kill experiment. CFUs were determined by manual counting, and all measurements are based on counts containing at least five colonies; we note here that a typical lower limit of quantification in our time-kill assays is between 1 to 10^2 CFU/mL, and, where applicable, we have truncated CFU/mL values according to the lower limit of quantification. Survival was determined by dividing all CFU/mL measurements to that immediately before antibiotic treatment at time 0 h.

Metabolic measurements. For all metabolic measurements in bulk culture, cells were diluted 1:100 from an overnight culture grown anaerobically into 50 mL Falcon tubes with working volumes of 50 mL. Cells were grown anaerobically for ~1.5 h at 37°C without shaking to early exponential phase, $OD_{600} \approx 0.02$. Antibiotics were added to the final concentrations indicated, and cultures were incubated without shaking at 37°C. After 20 min of treatment, cells were centrifuged at centrifuged at 3720 × *g* for 5 min, and washed with 500 μL PBS. Cells were centrifuged again at 1500 × *g* for 5 min, the supernatant was discarded, and 1 mL B-PER II (product 78260, Thermo Fisher Scientific, Waltham, MA) containing 100 μg/mL lysozyme (Sigma-Aldrich L6876) and 2.5 U/mL Dnase I (Thermo Fisher 90083) was added to each cell pellet for harvesting. Cells were incubated with vortexing for 10 min. Cells were then centrifuged again at 1500 × *g* for 5 min, and 800 μL of supernatant was aliquoted and removed from the anaerobic chamber for further analysis. Protein concentrations in the sample supernatants were determined using the Coomassie Plus protein assay reagent, as described below. Metabolite concentrations in the sample supernatants were determined using enzymatic assays. For these enzymatic assays, the supernatant was de-proteinized by aliquoting 500 μL of supernatant into a 10 kDa molecular weight cut-off (MWCO) spin filter (Thermo Fisher 88513), centrifuging at 12,000 × *g* for 30 min, and collecting the flow-through for analysis. The flow-through from B-PER II with lysozyme and DNAase (no cell lysate) was also collected for background determination during analysis.

Glucose concentration measurements. Glucose concentrations were measured using an enzymatic assay kit (Sigma-Aldrich MAK263). Standards of 0, 0.004, 0.008, 0.012, 0.016, and 0.02 nmole/μL glucose were generated, and 50 μL of standard or sample was added to each well

of a 96-well flat-bottom plate. 50 µL of the reaction mix comprising glucose assay buffer, glucose probe, and glucose enzyme mix were then added to each well following the manufacturer's instructions. The plate was incubated for 30 min at 37°C, protected from light. The fluorescence intensity at Ex/Em = 535/587 nm was measured using a SpectraMax M3 plate reader. Glucose concentration values were inferred by linearly interpolating fluorescence intensity values with respect to the standard curve.

Pyruvate concentration measurements. Pyruvate concentrations were measured using an enzymatic assay kit (Sigma-Aldrich MAK332). Standards of 0, 5, 10, 15, 20, 30, 40, and 50 µM pyruvate were generated, and 10 µL of standard or sample was added to each well of a 96-well flat-bottom plate. 90 µL of the reaction mix comprising enzyme mix and dye reagent were then added to each well following the manufacturer's instructions. The plate was incubated for 30 min at room temperature. The fluorescence intensity at Ex/Em = 530/585 nm was measured using a SpectraMax M3 plate reader. Pyruvate concentration values were inferred by linearly interpolating fluorescence intensity values with respect to the standard curve.

NADH and NAD^+ concentration measurements. NADH and total NADH and NAD^+ concentrations were measured using an enzymatic assay kit based on NAD cycling (product MET-5014, Cell Biolabs, San Diego, CA). In this assay, the concentrations of NADH, NAD^+, or total NADH and NAD^+ can be determined using an enzymatic cycling reaction in which NAD^+ is reduced to NADH, then NADH reacts with a probe that produces a colored product. NADH was specifically extracted, and NAD^+ was destroyed, by addition of NaOH. Briefly, 27.5 µL of each sample was added to a microcentrifuge tube, 5.5 µL of 0.1 N NaOH was added, and the tube was mixed. Tubes were incubated at 80°C for 1 h, protected from light. Tubes were centrifuged briefly to pool all sample solution, and 22 µL of the provided assay buffer was added to shift the pH back to neutral. The incubation with base was skipped for measurements of total NADH and NAD^+. pH in all samples was confirmed to be ~7.0 using pH test indicator strips (Sigma-Aldrich P4786). Standards of 0, 0.004, 0.008, 0.015, 0.031, 0.063, 0.125, 0.25, 0.5, and 1 µM NAD^+ were generated, and 50 µL of standard or sample was added to each well of a 96-well flat-bottom plate. 50 µL of the NAD cycling reagent comprising NAD cycling substrate, NAD cycling enzyme, colorimetric probe, and assay buffer was added to each well following the manufacturer's instructions. The plate was incubated for 3 h at room temperature, protected from light. The absorbance at 450 nm was measured using a SpectraMax M3 plate reader. NADH and total NADH and NAD^+ concentration values were inferred by linearly interpolating absorbance with respect to the standard curve, and NAD^+ values were determined by subtracting NADH values from total NADH and NAD^+ values.

Description of antibiotic-induced phenotypes. We have previously studied the cellular phenotypes induced by bactericidal antibiotics at the single-cell level (Wong et al. 2019; Wong et al. 2021a). In brief, salient phenotypes induced by aminoglycosides and fluoroquinolones include cytoplasmic condensation and lysis (Wong et al. 2021a), while salient phenotypes induced by β-lactams include membrane bulging and lysis (Yao et al. 2012; Wong et al. 2019; Wong et al. 2021b). Aminoglycoside- and fluoroquinolone-treated cells, treated with antibiotics for a timescale of hours, experience cytoplasmic condensation wherein discrete portions of the cellular cytoplasm become phase-light and the cell shrinks. This shrinkage occurs over a timescale of minutes, irreversibly halts cellular elongation, and has been evidenced to arise from

membrane damage (Wong et al. 2021a). Furthermore, we have previously shown that increases in the fluorescence intensities of carboxy-H_2DCFDA, DAF-FM, and C11-BODIPY occur coincident with cytoplasmic condensation and/or lysis in aminoglycoside- and fluoroquinolone-treated cells (Wong et al. 2021a). These cells remain condensed over a timescale of hours, until sudden lysis occurs (Wong et al. 2021a).

β-lactam-treated cells, treated with antibiotics for a timescale of tens of minutes, experience membrane bulging, wherein micron-sized, phase-dark membrane extrusions appear over the course of seconds. Cells remain bulged over a timescale of seconds to minutes, until sudden lysis occurs (Yao et al. 2012; Wong et al. 2019; Wong et al. 2021b). We have previously shown that membrane bulging can be explained by the formation of cell wall defects and the resulting elastic response of the cellular envelope (Wong et al. 2019; Wong et al. 2021b).

Microscopy. Microscopy experiments were performed with cells sandwiched between cover glasses and glass slides unless otherwise stated. Cells were concentrated by centrifugation at 2350 × *g* for 5 min and resuspended in a smaller volume of supernatant. We plated 1 to 2 μL of the resuspended bacterial culture on 3"×1"×1" microscope slides (product 125444, Fisher Scientific, Hampton, NH) containing LB-agarose pads for cell immobilization, and sealed the slides using 18 mm square cover glasses (product 48366, VWR, Radnor, PA). Cells were imaged immediately afterward. We used a Zeiss Axioscope A1 upright microscope equipped with a Zeiss Axiocam 503 camera and a Zeiss 100x NA 1.3 Plan-neofluar objective (Zeiss, Jena, Germany) located inside the anaerobic chamber. Images were recorded using Zen Lite Blue (Zeiss), and processed and analyzed using ImageJ (NIH, Bethesda, MD). When possible, epifluorescence exposure times were limited to a maximum of 300 ms to avoid photobleaching. All microscopy experiments were replicated at least twice, and we verified that the absolute values of all fluorescence intensities were comparable across experiments performed using this microscopy setup.

RMB detection with fluorescent dyes. All dyes below were added directly to cell cultures and incubated for at least 30 min before subsequent analyses. For general detection of oxidative stress and ROS (H_2O_2, $ROO\cdot$, and $ONOO^-$), we used the cell-permeant dye carboxy-H_2DCFDA (Invitrogen C400), which was dissolved in DMSO and added to incubating liquid cultures to a final concentration of 10 μM. As a positive control, cells were treated with 10 mM H_2O_2 (Sigma-Aldrich H1009) for the same durations as with antibiotics. For detection of RNS, in particular nitric oxide (NO), we used DAF-FM diacetate (Invitrogen D23844), dissolved in DMSO and added to incubating liquid cultures to a final concentration of 10 μM. As a positive control, we treated cells with 1 mM diethylamine NONOate (Sigma-Aldrich D184), which was dissolved in ethanol to prepare stock solutions, for the same durations as with antibiotics. C11-BODIPY 581/591 (Invitrogen D3861), a fluorescent dye-based lipid peroxidation sensor whose fluorescence emission peak shifts from red to green upon lipid peroxidation, was dissolved in DMSO and added to incubating liquid cultures to a final concentration of 10 μM to stain membranes undergoing lipid peroxidation. As a positive control, cells were treated with 10 mM H_2O_2 for the same durations as with antibiotics. For all samples, cellular phenotypes were manually determined with respect to corresponding phase contrast images. We note here that lysed cells may exhibit fluorescence, as indicated in Figure 2 of the main text: in such cells, despite large decreases in cytoplasmic phase contrast intensity accompanying cellular lysis, cytoplasmic material remained after lysis, and the remaining material retained some

fluorescence.

Exogenous RES. 4-HNE (product 32100, Cayman Chemical, Ann Arbor, MI) was supplied as a solution in ethanol, and 4-HNE controls were performed by adding ethanol to cells. MGO (Sigma-Aldrich M0252) was supplied as an aqueous solution. All of these reagents were freshly prepared or diluted before each experiment.

DNA double-strand break detection with GamGFP. DNA double-strand breaks (DSBs) were detected using an engineered fluorescent protein-based probe (Shee et al. 2013). This probe uses a fusion of GFP to the Gam protein from phage Mu that binds to DSBs when expressed in *E. coli*. We performed this experiment under anaerobic conditions as follows. An overnight culture of *E. coli* SMR14334, grown anaerobically, was diluted 1:100 in LB media containing 100 ng/mL doxycycline for GamGFP induction. At $OD_{600} \approx 0.02$, where applicable, cells were treated with the indicated compounds at the indicated concentrations. Cultures were incubated for the indicated times, and cells were analyzed using fluorescence microscopy as detailed above.

Membrane damage detection with SYTOX Blue. Membrane damage was detected using a membrane damage-sensitive dye, SYTOX Blue Nucleic Acid Stain (Invitrogen S11348), following previous work (Wong et al. 2021a). We performed this experiment under anaerobic conditions as follows. An overnight culture of *E. coli* MG1655, grown anaerobically, was diluted 1:100 in LB media. At $OD_{600} \approx 0.02$, cells were treated with SYTOX Blue at a final concentration of 10 μM and, where applicable, any additional indicated compounds at the indicated concentrations. Cultures were incubated for the indicated times, and cells were analyzed using fluorescence microscopy as detailed above.

Image analysis. Cells were counted manually to determine phenotypes, such as condensation and lysis. For RMB dye experiments, fluorescence was quantitatively analyzed with ImageJ (National Institutes of Health, Bethesda, MD). Closed cell contours were delineated based on phase contrast images and ImageJ was used to measure the mean fluorescence pixel intensity within a given contour. This was done both manually and using the MicrobeJ plugin (Ducret et al. 2016) for reproducible automation. The average background fluorescence intensity was subtracted from all measured values. Fractional fluorescence enhancement was calculated as the ratio of fluorescence intensities (1) inside a cell contour and (2) averaged over background regions with no cells. We were not blinded to allocation in the image analysis, and all cells for which we could reliably determine phenotypes or measure fluorescence intensities were used. For GamGFP and SYTOX Blue experiments, closed cell contours were delineated based on phase contrast images, and the respective quantification of foci-containing and fluorescently stained cells were performed manually and semi-automatically using ImageJ. We were not blinded to allocation in the image analysis, and cells for which we could reliably determine the presence or absence of foci or measure fluorescence intensities were used.

RMB scavengers. L-glutathione reduced (Sigma-Aldrich G4251), n-acetyl-l-cysteine (Sigma-Aldrich A9165), and pyridoxamine dihydrochloride (Sigma-Aldrich P9380) were dissolved in ultrapure Milli-Q water. All scavengers were freshly prepared before each experiment.

ATP abundance assay. Intracellular ATP was quantified using the BacTiter-Glo Microbial Cell

Viability Assay (product G8230, Promega, Madison, WI) according to the manufacturer's instructions. Luminescence and optical density (OD_{600}) of samples were measured with a SpectraMax M3 plate reader. For anaerobic cultures, cells were treated with the BacTiter-Glo assay solution inside the anaerobic chamber, incubated for at least 5 min for lysis, then removed from the anaerobic chamber for luminescence measurements performed immediately after removal, using a SpectraMax M3 microplate reader located outside the anaerobic chamber. As an additional positive control used for ATP/OD_{600} determination, cells cultured in Neidhardt EZ Rich Defined Medium (Teknova Inc., Hollister, CA) were noted to exhibit substantially increased ATP/OD_{600} levels ($ATP/OD_{600} \sim 7$) relative to cells cultured in LB only ($ATP/OD_{600} = 1$), and the former culture condition was included and assayed in parallel in all experiments.

Changes in membrane permeability and PMF. $DiBAC_4(3)$ (Invitrogen B438), a fluorescent reporter of membrane potential ($\Delta\Psi$), was dissolved in DMSO and added to incubating liquid cultures to a final concentration of 10 μg/mL to stain cells with and without depolarized membranes. ACMA (9-amino-6-chloro-2-methoxyacridine; Invitrogen A1324), a fluorescent reporter which binds to membranes in the energized state and becomes quenched if a pH gradient forms, was dissolved in DMSO and added to incubating liquid cultures to a final concentration of 10 μg/mL to assay changes in ΔpH. $DiSC_3(5)$ (Invitrogen D306), a fluorescent reporter which accumulates on hyperpolarized membranes and is translocated into the lipid bilayer, was dissolved in DMSO and added to incubating liquid cultures to a final concentration of 1 μM. As a positive control for $DiBAC_4(3)$ and ACMA, CCCP (carbonyl cyanide 3-chlorophenylhydrazone; Sigma-Aldrich C2759), a protonophore which uncouples PMF, was dissolved in DMSO and added to incubating liquid cultures at least 5 min before imaging, to a final concentration of 1 mM. As a positive control for $DiSC_3(5)$, valinomycin (Sigma-Aldrich V0627), an ionophore antibiotic, was dissolved in DMSO and added to incubating liquid cultures at least 5 min before imaging to a final concentration of 100 μg/mL.

Intracellular kanamycin concentration measurements. Intracellular kanamycin concentration measurements were performed using kanamycin-Texas Red analogously to previous work (Meylan et al. 2017; Sandoval et al. 1998). One milligram of Texas red sulfonyl chloride (Thermo Fisher T1905) was resuspended in 50 μL of anhydrous *N,N*-dimethylformamide (Sigma-Aldrich 227056) on ice. The solution was added to 2.3 mL of 100 mM K_2CO_3 (Sigma-Aldrich P5833) at pH 8.5, with or without 10 mg/mL kanamycin, on ice. To quantify kanamycin-Texas Red concentrations, 2 mL of cells was grown to log-phase anaerobically from a 1:100 dilution of an overnight culture to $OD_{600} \approx 0.02$, as described above. Concentrated kanamycin-Texas Red was then added to achieve a working concentration of 50 μg/mL, scavenger (10 mM final concentration) was added where applicable, and samples were incubated anaerobically for 1 h. Samples were then analyzed using fluorescence microscopy, as detailed above.

Preparation of samples for LC-MS. For each sample used to measure ciprofloxacin or mecillinam concentration, 100 mL of cells was grown to log-phase anaerobically from a 1:100 dilution of an overnight culture to $OD_{600} \approx 0.02$ without shaking and in 250-mL flasks. Cells were then treated with mecillinam at a final concentration of 10 μg/mL or ciprofloxacin at a final concentration of 1 μg/mL, and scavenger (10 mM final concentration) was added where applicable. After 4 h, 50 mL of cell culture was aliquoted, centrifuged at 3720 × *g* for 10 min, and washed with 500 μL PBS. Cells were centrifuged again at 1500 × *g* for 10 min, the

supernatant was discarded, and 500 µL acetonitrile (Sigma-Aldrich 271004) was added to the cell pellet. Mecillinam or ciprofloxacin concentrations in these samples were determined using liquid chromatography-mass spectrometry (LC-MS), as detailed below. The remaining 50 mL of cell culture was used for protein concentration determination, as detailed below.

Preparation of samples for GC-MS. For each sample used to measure RES concentration or protein concentration, at least 50 mL of log-phase bulk cultures of *E. coli* MG1655 grown in LB were treated with kanamycin, ciprofloxacin, and mecillinam at the indicated concentrations for the indicated times in 250-mL flasks. Cells were then aliquoted into 50 mL Falcon tubes. Tubes were centrifuged at 3720 × *g* for 10 min. Next, we discarded the supernatant in all samples. Each cell pellet was washed with 500 µL PBS, resuspended, and centrifuged at 1500 × *g* for 10 min. Afterward, the supernatant was discarded from each sample.

For samples used in RES concentration determination and protein concentration determination, 1 mL B-PER II containing 100 µg/mL lysozyme, 5 U/mL DNase I, and 25 mM *O*-(2,3,4,5,6-Pentafluorobenzyl)hydroxylamine (PFBHA; Sigma-Aldrich 76735) as a carbonyl derivatizing agent was then added to cell pellets for harvesting, and, as an internal standard, deuterated benzaldehyde (benzaldehyde-d_6, product D-0005, CDN Isotopes, Pointe-Claire, Quebec, Canada) was added to the lysis buffer to a final concentration of 100 µM immediately before dispensing of the lysis buffer to cell pellets. The same lysis buffer without PFBHA and deuterated benzaldehyde was used for protein concentration determination of samples from cell cultures that were processed using LC-MS to measure ciprofloxacin and mecillinam concentrations.

After addition of lysis buffer, all samples were vortexed and incubated at 37°C for 30 minutes. All samples were then centrifuged at 1500 × *g* for 10 min, and the supernatant was aliquoted from each sample for further analysis of RES or protein concentrations. For RES measurements, the supernatants were removed from the anaerobic chamber at this point, flash-frozen on dry ice, and stored at -80°C until processing at the Harvard Center for Mass Spectrometry.

Protein concentration assay. We used the Coomassie Plus protein assay reagent (Thermo Fisher 23236) following the manufacturer's instructions. This measurement was performed under aerobic conditions using the supernatants prepared under anaerobic conditions. Briefly, for each sample, 10 µL of sample was pipetted directly into 300 µL of Coomassie Plus reagent in a 96-well plate. The plate was mixed and incubated at room temperature for 10 minutes, and the absorbance at 595 nm was read with a SpectraMax M3 spectrophotometer. Standard curves were generated from control samples with bovine serum albumin (BSA) concentrations of 2000, 1500, 1000, 750, 500, 250, 125, 25, and 0 µg/mL, where BSA was diluted in the same lysis buffer used to prepare samples. Protein concentration values were inferred by linearly interpolating absorbance values with respect to the standard curves.

GC-MS. GC-MS experiments were performed at the Harvard Center for Mass Spectrometry. Cell lysates were analyzed for target derivatives of PFBHA with 4-HNE and MGO. All samples were run on a Thermo GC-QE mass spectrometer using an Agilent DB-5MS (30 m, 0.25 mm diameter, 0.25 µm film) column with the following orbitrap parameters: polarity, pos; resolution, 60000; agc target, 1e6; scan range, 66.7 to 1000 *m/z*. Samples were injected in splitless mode. The GC oven was maintained at 50°C for 4 min, before increasing to 300°C at 15°C/min and

finally maintained at 300°C for 24 min. Cell lysate samples were prepared as follows. Between 750 to 800 µL of each sample was transferred to a new tube, then 500 µL of methanol was added to each sample. Samples were transferred to 8 mL glass vials and incubated at room temperature for 30 min. 1 mL of hexane was added, and samples were vortexed for 1 min. Six drops of sulfuric acid were added, and then samples were again vortexed for 1 min. Samples were centrifuged at 2500 × *g*, the supernatant was transferred to glass autosampler vials while avoiding the aqueous phase, and the samples were dried under flow of N_2. Finally, the samples were resuspended in 50 µL hexane, and 45 µL of the suspension was transferred to microinserts (the remaining 5 µL being used to test pH). Standards were prepared as a 100 µM solution of 4-HNE and MGO in lysis buffer containing internal standard, and six 1/5 dilution series of each standard were subsequently prepared. 1 mL of each standard was then transferred to 8 mL vials, 500 µL of methanol was added to each standard, and standards were then treated like samples.

Benzaldehyde-d_6 was used as an internal standard, yielding a fragment at *m/z* = 181.0069. The following accurate *m/z* of fragment ions were used for quantification: 250.0287 for 4-HNE, 265.0396 for MGO, and 181.0069 for the internal standard. The quantification was based on the ratio with the internal standard area. Samples with low internal standard signals were not used. The limits of detection for 4-HNE and MGO in this protocol were 0.64 pmol and 16 pmol, respectively. Sample chromatograms for standards and chemical structures of target derivatives are shown in Figure S3. Most GC-MS measurements were performed on two independent occasions, and typical values are reported as fold changes to facilitate comparison.

Intracellular ciprofloxacin concentration LC-MS. In previous work (Gutierrez et al. 2017; Asuquo et al. 1993), intracellular ciprofloxacin concentrations were assayed fluorometrically with Ex/Em in the range of 275/410 nm. However, the addition of exogenous scavengers may interfere with this fluorometric reading: pyridoxamine, for instance, has Ex/Em in the range of 335/400 nm (Sikorska et al. 2004). We therefore quantified intracellular ciprofloxacin concentrations using LC-MS experiments, which were performed at the Harvard Center for Mass Spectrometry. Deuterated ciprofloxacin, ciprofloxacin-d_8 (product 25466, Cayman Chemical Company, Ann Arbor, MI), was used as an internal standard. All solvents used are LC-MS grade. 100 µL of ciprofloxacin-d_8 in acetonitrile was added to thawed samples. Samples were vortexed for 1 min, until the cell pellets were fully resuspended; an ultrasound bath was used, if needed, to loosen the pellets. Samples were then incubated in an ultrasound bath for 30 min, centrifuged at maximum speed for 10 min, transferred to new microcentrifuge tubes, dried under N_2 flow, and resuspended in 100 µL of acetonitrile (50% in water).

A standard curve was prepared using eight 1/5 dilution series of a 100 µM solution of ciprofloxacin in acetonitrile containing internal standard. Standards were prepared similarly to the samples. The lower limit of quantification was found to be less than 1.28 nM.

All samples were run on a Thermo QE+. The column used was Phenomenex Kinetex C18, 1.7 µm, 100 Å, 150 × 2.1 mm. The source used was HESI+. MS parameters were as follows: full MS 200-600 *m/z*, resolution 70000, 100 ms max IT, 3e6 AGC. The mobile phases were A: water, 0.1% formic acid, 5 mM ammonium formate and B: acetonitrile. The following gradient was used: 3 min at 10% B, then to 100% B in 0 min, followed by 7 min at 100% B. The column was then equilibrated at 10% B for 3 min. The flow rate was 0.25 mL/min. Each sample was injected twice continuously, and the second injections were used for quantification.

Intracellular mecillinam concentration LC-MS. LC-MS experiments were performed at the

Harvard Center for Mass Spectrometry. Deuterated ampicillin, ampicillin-d_5 (Cayman Chemical 25356), was used as an internal standard. All solvents used are LC-MS grade. 300 µL of acetonitrile and internal standard (ampicillin-d_5 at 0.33 µM) was added to frozen samples. 200 µL of H_2O was added, and samples were left to thaw. Samples were vortexed for 30 s, and then incubated in an ultrasound bath for 30 min. Samples were then centrifuged at max speed for 20 min, transferred to new tubes, dried under N_2 flow, and resuspended in 100 µL of acetonitrile (50% in water).

A standard curve was prepared using nine 1/5 dilution series of a 1 mM solution of mecillinam in LB. 50 µL of each standard was prepared similarly to the samples. The lower limit of quantification was found to be 2.5 nM.

All samples were run on an Agilent 6460 Triple Quad Mass Spectrometer coupled to a 1290 LC. The column used was Phenomenex Kinetex C18, 1.7 µm, 100 Å, 150 × 2.1 mm. The source used was ESI turbojet, with gas temperature 330°C, gas flow 8L/min, nebulizer 40 psi, sheath gas 375°C at 9L/min, capillary at +2800 V and nozzle at +300 V, and delta EMV of +100. The mobile phases were A: water, 0.1% formic acid and B: acetonitrile, 0.1% formic acid. The following gradient was used: 5 min at 0% B, then to 100% B in 10 min, followed by 5 min at 100% B. The column was then equilibrated at 0% B for 5 min. The flow rate was 0.2 mL/min. Each sample was injected twice continuously with the exception of two samples, and resulting measurements of mecillinam concentration were averaged. The two samples that were not injected twice continuously were injected only once each: these were both samples corresponding to treatment with mecillinam and pyridoxamine, and the mecillinam concentrations in these samples were found to be within 10% of variation.

QUANTIFICATION AND STATISTICAL ANALYSIS

Statistical parameters were reported either in individual figures or corresponding figure legends. Two-sample Kolmogorov-Smirnov tests or two-sample *t*-tests for differences in mean value, as indicated in each figure where applicable, were performed at the standard 5% significance level. We were not blinded to allocation in the statistical testing. All statistical analyses were performed using MATLAB.

References

Allocati, N., Federici, L., Masulli, M. & Di Ilio, C. Glutathione transferases in bacteria. *FEBS J.* **276**, 58-75 (2009).

Amarnath, V., Amarnath, K., Amarnath, K., Davies, S. & Roberts, L. J. Pyridoxamine: an extremely potent scavenger of 1,4-dicarbonyls. *Chem. Res. Toxicol.* **17**, 410-415 (2004).

Aquillano, K., Baldelli, S., and Ciriolo, M. R. Glutathione: new roles in redox signaling for an old antioxidant. *Front. Pharmacol.* **5**, 196 (2014).

Asuquo, A. E. & Piddock, L. J. Accumulation and killing kinetics of fifteen quinolones for *Escherichia coli, Staphylococcus aureus,* and *Pseudomonas aeruginosa*. *J. Antimicrob. Chemother.* **31,** 865-880 (1993).

Baba, T. et al. Construction of *Escherichia coli* K-12 in-frame, single-gene knockout mutants: the Keio collection. *Mol. Syst. Biol.* **2,** 2006.0008 (2006).

Belenky, P. et al. Bactericidal antibiotics induce toxic metabolic perturbations that lead to cellular damage. *Cell Rep*. **13**, 968–980 (2015).

Blokhina, O. B., Chirkova, T. V. & Fagerstedt, K. V. Anoxic stress leads to hydrogen peroxide formation in plant cells. *J. Exp. Bot.* **52**, 1179-1190 (2001).

Brynildsen, M. P., Winkler, J. A., Spina, C. S., MacDonald, I. C. & Collins, J. J. Potentiating antibacterial activity by predictably enhancing endogenous microbial ROS production. *Nat. Biotechnol.* **31**, 160–165 (2013).

Chan, K., Poon, R. & O'Brien, P. J. Application of structure–activity relationships to investigate the molecular mechanisms of hepatocyte toxicity and electrophilic reactivity of α,β-unsaturated aldehydes. *J. Appl. Toxicol.* **28**, 1027-1039 (2008).

Crane, B. R., Sudhamsu, J. & Patel, B. A. Bacterial nitric oxide synthases. *Annu. Rev. Biochem.* **79**, 445–470 (2010).

Csala, M. et al. On the role of 4-hydroxynonenal in health and disease. *Biochim. Biophys. Acta.* **1852**, 826-838 (2015).

Dalleau, S., Baradat, M., & Huc, L. Cell death and diseases related to oxidative stress:4-hydroxynonenal (HNE) in the balance. *Cell Death Differ.* **20,** 1615-1630 (2013).

Datsenko, K. A. & Wanner, B. L. One-step inactivation of chromosomal genes in *Escherichia coli* K-12 using PCR products. *Proc. Natl. Acad. Sci.* **97,** 6640-6645 (2000).

Davies, B. W. et al. Hydroxyurea induces hydroxyl radical-mediated cell death in *Escherichia coli. Mol. Cell* **36**, 845–860 (2009).

Deponte, M. The incomplete glutathione puzzle: just guessing at numbers and figures? *Antioxid. Redox Signal.* **27**, 1130-1161 (2017).

Dowhan, W. Molecular basis for membrane phospholipid diversity: why are there so many lipids? *Annu. Rev. Biochem.* **66,** 199-232 (1997).

1203 Drlica, K. & Zhao, X. Bacterial death from treatment with fluoroquinolones and other lethal
1204 stressors. *Expert Rev. Anti. Infect. Ther.* 1-18 (2020).

1205 Ducret, A., Quardokus, E. M., & Brun, Y. V. MicrobeJ, a tool for high throughput bacterial cell
1206 detection and quantitative analysis. *Nat. Microbiol.* **1**, 16077 (2016).

1207 Dwyer, D. J. et al. Antibiotics induce redox-related physiological alterations as part of their
1208 lethality. *Proc. Natl. Acad. Sci. USA* **111**, E2100–E2109 (2014).

1209 Dwyer, D. J., Camacho, D. M., Kohanski, M. A., Callura, J. M. & Collins, J. J. Antibiotic-
1210 induced bacterial cell death exhibits physiological and biochemical hallmarks of apoptosis. *Mol.*
1211 *Cell* **46**, 561–572 (2012).

1212 Dwyer, D. J., Kohanski, M. A., Hayete, B. & Collins, J. J. Gyrase inhibitors induce an oxidative
1213 damage cellular death pathway in *Escherichia coli*. *Mol. Syst. Biol.* **3**, 91 (2007).

1214 Ezraty, B. et al. Fe-S cluster biosynthesis controls uptake of aminoglycosides in a ROS-less
1215 death pathway. *Science* **340**, 1583-1587 (2013).

1216 Ferguson, G. P. et al. Protection of the DNA during the exposure of *Escherichia coli* cells to a
1217 toxic metabolite: the role of the KefB and KefC potassium channels. *Mol. Microbiol.* **35**, 113-
1218 122 (2000).

1219 Ferguson, G. P. Protective mechanisms against toxic electrophiles in *Escherichia coli. Trends*
1220 *Microbiol.* **7**, 242-247 (1999).

1221 Foti, J. J., Devadoss, B., Winkler, J. A., Collins, J. J. & Walker, G. C. Oxidation of the guanine
1222 nucleotide pool underlies cell death by bactericidal antibiotics. *Science* **336**, 315–319 (2012).

1223 Freedberg, W. B., Kistler, W. S., and Lin, E. C. C. Lethal synthesis of methylglyoxal by
1224 *Escherichia coli* during unregulated glycerol metabolism. *J. Bact.* **108**, 137-144 (1971).

1225 Garvey, N., St. John, A. C., & Witkin, E. M. Evidence for RecA protein association with the cell
1226 membrane and for changes in the levels of major outer membrane proteins in SOS-induced
1227 *Escherichia coli* cells. *J. Bacteriol.* **163,** 870-876 (1985).

1228 Girgis, H. S., Harris, K., & Tavazoie, S. Large mutational target size for rapid emergence of
1229 bacterial persistence. *Proc. Natl. Acad. Sci. USA* **109,** 12740-12745 (2012).

1230 Girgis, H. S., Hottes, A. K., & Tavazoie, S. Genetic architecture of intrinsic antibiotic
1231 susceptibility. *PLoS ONE* **4,** e5629 (2009).

1232 Giroux, X., Su, W.-L., Bredeche, M.-F., & Matic, I. Maladaptive DNA repair is the ultimate
1233 contributor tothe death of trimethoprim-treated cells under aerobic and anaerobic conditions.
1234 *Proc. Natl. Acad. Sci. USA* **114,** 11512-11517 (2017).

1235 Goswami, M., Subramanian, M., Kumar, R., Jass, J. & Jawali, N. Involvement of antibiotic
1236 efflux machinery in glutathione-mediated decreased ciprofloxacin activity in *Escherichia coli.*
1237 *Antimicrob. Agents Chemother.* **60,** 4369-4374 (2016).

1238 Grant, S. S., Kaufmann, B. B., Chand, N. S., Haseley, N. & Hung, D. T. Eradication of bacterial
1239 persisters with antibiotic-generated hydroxyl radicals. *Proc. Natl. Acad. Sci. USA* **109**, 12147–
1240 12152 (2012).

Gusarov, I., Shatalin, K., Starodubtseva, M., and Nudler, E. Endogenous nitric oxide protects bacteria against a wide spectrum of antibiotics. *Science* **325**, 1380-1384 (2009).

Gutierrez, A. et al. β-lactam antibiotics promote bacterial mutagenesis via an RpoS-mediated reduction in replication fidelity. *Nat. Commun.* **4,** 1610 (2013).

Gutierrez, A. et al. Understanding and sensitizing density-dependent persistence to quinolone antibiotics. *Mol. Cell* **68,** 1147-1154 (2017).

Hajjar, C. et al. The NOX family of proteins is also present in bacteria. *mBio* **8**, e01487-17 (2017).

Hansen, M. C., Palmer, R. J., Udsen, C., White, D. C. & Molin, S. Assessment of GFP fluorescence in cells of Streptococcus gordonii under conditions of low pH and low oxygen concentration. *Microbiology* **147,** 1383-1391 (2001).

Hong, R., Kang, T. Y., Michels, C. A., and Gadura, N. Membrane lipid peroxidation in copper alloy-mediated contact killing of *Escherichia coli*. *Appl. Environ. Microbiol.* **78**, 1776-1784 (2012).

Hong, Y., Zeng, J., Wang, X., Drlica, K. & Zhao, X. Post-stress bacterial cell death mediated by reactive oxygen species. *Proc. Natl. Acad. Sci. USA* **116**, 10064–10071 (2019).

Imlay, J. A. Diagnosing oxidative stress in bacteria: not as easy as you might think. *Curr. Opin. Micobiol.* **24**, 124-131 (2015).

Kawai, Y. et al. Crucial role for central carbon metabolism in the bacterial L-form switch and killing by β-lactam antibiotics. *Nat. Microbiol.* **4**, 1716-1726 (2019).

Keren, I., Wu, Y., Inocencio, J., Mulcahy, L. R. & Lewis, K. Killing by bactericidal antibiotics does not depend on reactive oxygen species. *Science* **339**, 1213–1216 (2013).

Khakimova, M. et al. The stringent response controls catalases in *Pseudomonas aeruginosa* and is required for hydrogen peroxide and antibiotic tolerance. *J. Bacteriol.* **195,** 2011-2020 (2013).

Kohanski, M. A., Dwyer, D. J. & Collins, J. J. How antibiotics kill bacteria: from targets to networks. *Nat. Rev. Microbiol.* **8**, 423–435 (2010).

Kohanski, M. A., DePristo, M. A, & Collins, J. J. Sublethal antibiotic treatment leads to multidrug resistance via radical-induced mutagenesis. *Mol. Cell* **12,** 311-320 (2010).

Kohanski, M. A., Dwyer, D. J., Hayete, B., Lawrence, C. A. & Collins, J. J. A common mechanism of cellular death induced by bactericidal antibiotics. *Cell* **130**, 797–810 (2007).

Lee, C. and Park, C. Bacterial responses to glyoxal and methylglyoxal: reactive electrophilic species. *Int. J. Mol. Sci.* **18**, 169 (2017).

Liu, W., Porter, N. A., Schneider, C., Brash, A. R. & Yin, H. Formation of 4-hydroxynonenal from cardiolipin oxidation: intramolecular peroxyl radical addition and decomposition. *Free Radic. Biol. Med.* **50,** 166-178 (2011).

Liu, Y. & Imlay, J. A. Cell death from antibiotics without the involvement of reactive oxygen species. *Science* **339**, 1210–1213 (2013).

Lo, T. W. C., Westwood, M. E., McLellan, A. C., Selwood, T. and Thornalley, P. J. Binding and modification of proteins by methylglyoxal under physiological conditions. *J. Biol. Chem.* **269**, 32299-32305 (1994).

Lobritz, M. A. et al. Antibiotic efficacy is linked to bacterial cellular respiration. *Proc. Natl. Acad. Sci. USA* **112**, 8173-8180 (2015).

Lopatkin, A. et al. Clinically relevant mutations in core metabolic genes confer antibiotic resistance. *Science* **371**, eaba0862 (2021).

Lopatkin, A. J. et al. Bacterial metabolic state more accurately predicts antibiotic lethality than growth rate. *Nat. Microbiol.* **4**, 2109–2117 (2019).

Luo, X. P. et al. Determination of aldehydes and other lipid peroxidation products in biological samples by gas chromatography-mass spectrometry. *Anal. Biochem.* **228,** 294-298 (1995).

Luo, Y. & Helmann, J. D. Analysis of the role of *Bacillus subtilis* σ^M in β-lactam resistance reveals an essential role for c-di-AMP in peptidoglycan homeostasis. *Mol. Microbiol.* **83,** 623-639 (2012).

Martin, N. L. & Beveridge, T. J. Gentamicin interaction with *Pseudomonas aeruginosa* cell envelope. *Antimicrob. Agents Chemother.* **29,** 1079-1087 (1986).

Mathieu, A. et al. Discovery and function of a general core hormetic stress response in *E. coli* induced by sublethal concentrations of antibiotics. *Cell Rep.* **17,** 46-57 (2016).

Meylan, S. et al. Carbon sources tune antibiotic susceptibility in *Pseudomonas aeruginosa* via tricarboxylic acid cycle control. *Cell Chem. Biol.* **24,** 195-206 (2017).

Mironov, A. et al. Mechanism of H_2S-mediated protection against oxidative stress in *Escherichia coli*. *Proc. Natl. Acad. Sci. USA* **114**, 6022-6027 (2017).

Morones-Ramirez, J. R., Winkler, J. A., Spina, C. S. & Collins, J. J. Silver enhances antibiotic activity against Gram-negative bacteria. *Sci. Transl. Med*. **5**, 190ra81 (2013).

Nagaraj, R. H. et al. Effect of pyridoxamine on chemical modification of proteins by carbonyls in diabetic rats: characterization of a major product from the reaction of pyridoxamine and methylglyoxal. *Arch. Biochem. Biophys.* **402**, 110-119 (2002).

Negre-Salvayre, A., Coatrieux, C., Ingueneau, C. & Salvayre, R. Advanced lipid peroxidation end products in oxidative damage to proteins. Potential role in diseases and therapeutic prospects for the inhibitors. *Br. J. Pharmacol.* **153**, 6-20 (2008).

Nguyen, D. et al. Active starvation responses mediate antibiotic tolerance in biofilms and nutrient-limited bacteria. *Science* **334,** 982-986 (2011).

Nishida, M. et al. Hydrogen sulfide anion regulates redox signaling via electrophile sulfhydration. *Nat. Chem. Biol.* **8**, 714-724 (2012).

Ohsawa, I. et al. Hydrogen acts as a therapeutic antioxidant by selectively reducing cytotoxic oxygen radicals. *Nat. Med.* **13,** 688-694 (2007).

1314 Pribis, J. P. et al. Gamblers: an antibiotic-induced evolvable cell subpopulation differentiated by
1315 reactive-oxygen-induced general stress response. *Mol. Cell* **74,** 785-800 (2019).

1316 Reddy, C. A. et al. *Methods for General and Molecular Microbiology.* ASM Press (2007).

1317 Sandoval, R., Leiser, J., & Molitoris, B. A. Aminoglycoside antibiotics traffic to the Golgi
1318 complex in LLC-PK1 cells. *J. Am. Soc. Nephrol.* **9,** 167-174 (1998).

1319 Shatalin, K. et al. H_2S: A universal defense against antibiotics in bacteria. *Science* **334**, 986-990
1320 (2011).

1321 Shee, C. et al. Engineered proteins detect spontaneous DNA breakage in human and bacterial
1322 cells. *eLife* **2,** e01222 (2013).

1323 Sikorska, E., Górecki, T., Khmelinskii, I. V., Sikorski, M., & De Keukeleire, D. Fluorescence
1324 spectroscopy for characterization and differentiation of beers. *J. Inst. Brew.* **110,** 267-275 (2004).

1325 Stokes, J. M., Lopatkin, A. J., Lobritz, M. A. & Collins, J. J. Bacterial metabolism and antibiotic
1326 efficacy. *Cell Metab*. **30**, 30312–2 (2019).

1327 Takahashi, N. et al. Lethality of MalE-LacZ hybrid protein shares mechanistic attributes with
1328 oxidative component of antibiotic lethality. *Proc. Natl. Acad. Sci. USA* **114**, 9164-9169 (2017).

1329 Voziyan, P. A. & Hudson, B. G. Pyridoxamine: the many virtues of a maillard reaction inhibitor.
1330 *Ann. N. Y. Acad. Sci.* **1043**, 807-816 (2005).

1331 Wang, X. & Zhao, X. Contribution of oxidative damage to antimicrobial lethality. *Antimicrob.*
1332 *Agents. Chemother.* **53,** 1395-1402 (2009).

1333 Winterbourn, C. C. & Metodiewa, D. Reactivity of biologically important thiol compounds with
1334 superoxide and hydrogen peroxide. *Free Rad. Biol. Med.* **27,** 322-328 (1999).

1335 Wong, F. et al. Cytoplasmic condensation induced by membrane damage is associated with
1336 antibiotic lethality. *Nat. Commun.* **12**, 2321 (2021).

1337 Wong, F. et al. Understanding beta-lactam-induced lysis at the single-cell level. *Front.*
1338 *Microbiol.* **12**, 712007 (2021).

1339 Wong, F. and Amir, A. Mechanics and dynamics of bacterial cell lysis. *Biophys. J.* **116**, 2378-
1340 2389 (2019).

1341 Yang, J. H. et al. A white-box machine learning approach for revealing antibiotic mechanisms of
1342 action. *Cell* **177**, 1649-1661 (2019).

1343 Yao, Z., Kahne, D. & Kishony, R. Distinct single-cell morphological dynamics under beta-
1344 lactam antibiotics. *Mol. Cell* **48**, 705-712 (2012).

1345 Yeom, J., Imlay, J. A., & Park, W. Iron homeostasis affects antibiotic-mediated cell death in
1346 *Pseudomonas* species. *J. Biol. Chem.* **285,** 22689-22695 (2010).

1347 Yim, H.-S., Kang, S.-O., Hah, Y.-C., Chock, P. B., and Yim, M. B. Free radicals generated
1348 during the glycation reaction of amino acids by methylglyoxal. A model study of protein-cross-
1349 linked free radicals. *J. Biol. Chem.* **270**, 28228-28233 (1995).

Yin, H. Xu, L., & Porter, N. A. Free radical lipid peroxidation: mechanisms and analysis. *Chem. Rev.* **111,** 5944-5972 (2011).

Zhitkovich, A. *N*-Acetylcysteine: antioxidant, aldehyde scavenger, and more. *Chem. Res. Toxicol.* **32**, 1318-1319 (2019).

Zhu, Y., Eiteman, M. A., Altman, R., & Altman, E. High glycolytic flux improves pyruvate production by a metabolically engineered *Escherichia coli* strain. *Appl. Environ. Microbiol.* 74, 6649-6655 (2008).